gold-conjugated goat anti-mouse) and rabbit anti-laminin 5 (polyclonal highlighted by 15-nm gold-conjugated goat anti-rabbit; Biocell) were used. Sections were washed twice in TBS buffer and twice in distilled water (5 min each). After staining with 15% alcoholic uranyl acetate (3 min) and lead citrate (15 min), sections were observed with a transmission electron microscope (H-7100; Hitachi). Controls included normal skin sections with the primary antibody substituted by PBS, myeloma supernatant, preimmune rabbit serum, or an irrelevant immunoglobulin isotype, as a negative control. All experiments were performed in triplicate.

Immunogold Quantitative Analysis

The techniques for ultrastructural labeling were similar to those performed by McMillan et al. (2003b). Electron micrographs were taken at a standard magnification (30K) and were enlarged by a standard factor ×2.08. The final magnification (×62,500) was checked using electron micrographs taken of a carbon diffraction grating. For standardization purposes, all observations were made by one observer (JRM). At least 200 gold particles were assessed per specimen for each antibody or antiserum and four specimens from different individuals were examined (see Table 1 and Table 2). A 5-nm immunogold-conjugated final antibody layer was used. The percentage of gold particles perpendicularly beneath an observable electron-dense HD cytoplasmic outer attachment plaque as described by McMillan and Eady (1996) was scored and calculated from a large number of gold particles in skin from four individuals.

Only non-obliquely sectioned areas of dermal–epidermal junction were included with clearly defined HD plaques, lamina lucida (LL), and lamina densa (LD). The dermal–epidermal junction beneath melanocytes or in damaged areas was excluded from this study. Gold particles that appeared clumped or associated with any deposit were excluded.

For each antibody or antisera, the positions of gold particles were statistically tested by one-way ANOVA and a two-sample *t*-test using the Minitab statistical package (Minitab Inc; University of Pennsylvania, Philadelphia, PA). An antibody (4C7) that recognizes a carboxyl terminal domain of the α5 chain of laminins 10/11 was used to determine the mean position of labeling directly beneath the keratinocyte plasma membrane (Engvall et al. 1986; Makino et al. 2002)(see Figure 1 for epitope position). The labeling of the α5 chain was compared with the distribution of the G1 domain of laminin-5 α3 chain (using data previously reported by McMillan et al. 2003b).

Results

Confocal Fluorescence Microscopy of Control Skin

Laminin-5 staining was restricted to the dermal–epidermal junction in control skin (data not shown). This was similar to the dermal–epidermal junction staining of α5 chain of laminins 10 (data not shown). Laminins 10 and 11 were also expressed in dermal blood vessels. Laminin 11 (as identified by the β2 chain) dermal–epidermal junction staining was present in adult control thigh and arm skin but was variable in other samples including scalp skin. Therefore, β2 chain expression appears to be distinct and independent from that of the α5 chain. Staining for the α5, β1, and γ1 chains was weaker in the adult dermal–epidermal junction than in blood vessels (data not shown), whereas dermal–epidermal junction staining was generally brighter in younger skin samples (<16 years, data not shown). This would appear to support a previous report of age-dependent expression of the laminin 10/11 chains (Pouliot et al. 2002).

Confocal fluorescence microscopy (Figures 2A–2C) showed that both laminin-5 and α5 chains are expressed in the dermal–epidermal junction of control interfollicular epidermis except for small gaps (white arrows in Figures 2A and 2B) beneath small isolated cells presumed to be melanocytes staining blue for the melanocyte marker, TMH-1 (Figures 2A and 2B) (Masunaga et al. 1996). These data suggest that laminin-10 chains are restricted to beneath keratinocytes and are not expressed beneath melanocytes.

A previous scalp skin and hair follicle immunohistochemical study (Akiyama et al. 1995) demonstrated a specific staining pattern for many HD and anchoring filament components, particularly laminin 5, which manifests as reduced staining around the lower hair bulb and a reemergence of staining over the dermal papilla region (Akiyama et al. 1995). We observed this

Table 2 Immunogold particle distribution shows the majority of laminin labeling is restricted to beneath the hemidesmosome (HD) plaque

Antibody/antisera	Recognizes chain and epitope	Present in which chain/isoform(s)	Number of skin samples	Frequency of gold particles under HDs % (±SD)
Laminin 5	All chains[a]	Lam 5[a]	2[a]	77–88[a]
BM-165	α3 chain	Lam 5/6	4	82.65 (±3.87)
4C7	α5 chain	Lam 10/11	4	84.3 (±3.89)
2E8	β1 chain	Lam 6/10	4	91.7 (±3.99)
C4	β2 chain	Lam 7/11	4	88.4 (±3.56)
D18	γ1 chain	Lam 6/7/10/11	4	92.0 (±2.65)
M3F7	Collagen IV	α1/α2 helical (IV)	4	61.3 (±3.05)

[a]Data from McMillan et al. 2003b and Masunaga et al. 1996.

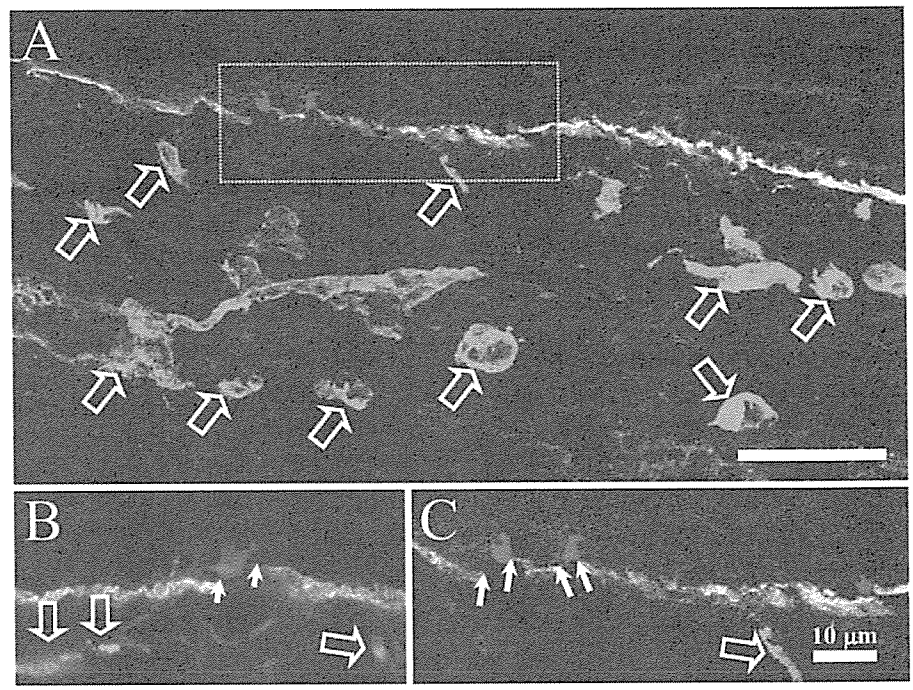

Figure 2 Reduced laminin 10 (green, FITC) and laminin 5 (red, Texas Red) labeling below the melanocyte marker TMH-1 (blue, CY-5) of normal adult control skin. Both laminin 5 and the α5 chain colocalize (orange color) within the dermal–epidermal junction (**A**) and both are expressed only weakly or are absent beneath melanocytes (**B,C**, in blue, see white arrows). The α5 chain of laminins 10/11 together with laminin 5 is not expressed beneath melanocytes (**A–C**, white arrows) but does show a distinct, strong expression pattern that includes dermal vessels (**A–C**, open arrows). Bar = 25 μm; Inset **C** = 10 μm.

characteristic pattern of staining along the majority of the follicles, for both laminin 5 (bracketed area in Figure 3A) and the laminin α5 chain (brackets and dotted line in Figures 3B and 3D). The laminin β1 and γ1 chains also showed this staining pattern (data not shown). There was no staining for the β2 chain in the hair follicle (data not shown). The dermal–epidermal junction of the bulge region stained for both α3 and the α5 chains (Figures 3A and 3B, Bu) and the α5 chain also stained the erector pili muscle (Figure 3C, EP).

Confocal Fluorescence Microscopy of Epidermolysis Bullosa Skin

The expression of laminins 5 (γ2 chain), 10 (all chains), and 11 (β2 chain) in patients with different forms of EB

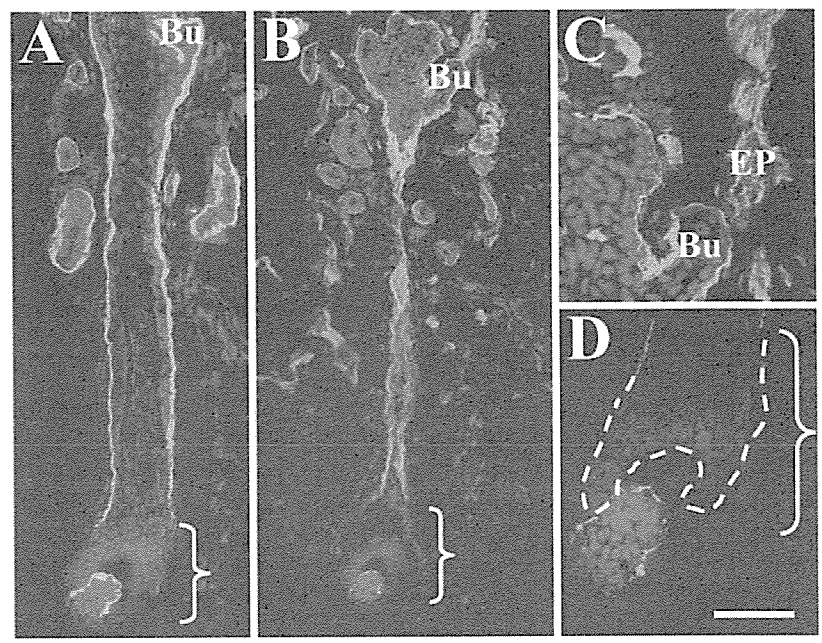

Figure 3 Indirect immunofluorescence shows a typical hemidesmosomal (HD) component-like expression pattern of the laminin α5 chain in late anagen human hair follicles. A previous scalp hair follicle immunohistochemical study (Akiyama et al. 1995) demonstrated a specific staining pattern for many HD-anchoring filament-associated components including laminin 5. In our study, both laminin-5 polyclonal staining (**A**) and the laminin α5 chain (**B**, 4C7) showed characteristic bright patterns along the epidermal proximal hair shaft including the bulge region (**B,C**, Bu) but progressively weaker staining toward the hair bulb (**D**, bracketed areas) with staining becoming brighter again higher up the hair shaft. Laminin α5 chain staining was present in the shaft (**B**) bulge region (**B,C**) and the apical tip of the hair bulb matrix (**D**). Laminin β1 and γ1 chains showed similar staining to the α5 chain (data not shown). No laminin β2 chain staining was detected in the hair follicle (data not shown). Bar = 25 μm.

was compared. In both control (Figure 4A) and all of the EB subtypes (Figures 4B–4H), α5, β1, β2, and γ1 chain expression was detectable. Laminin expression was weak in areas of split skin particularly in HJEB with defects in laminin 5 (α5 chain, Figures 4B and 4C, respectively, asterisks show the split area) (Uitto and Pulkkinen 2001). The reduction in α5 and β2 chain expression in HJEB patients, particularly over split skin,

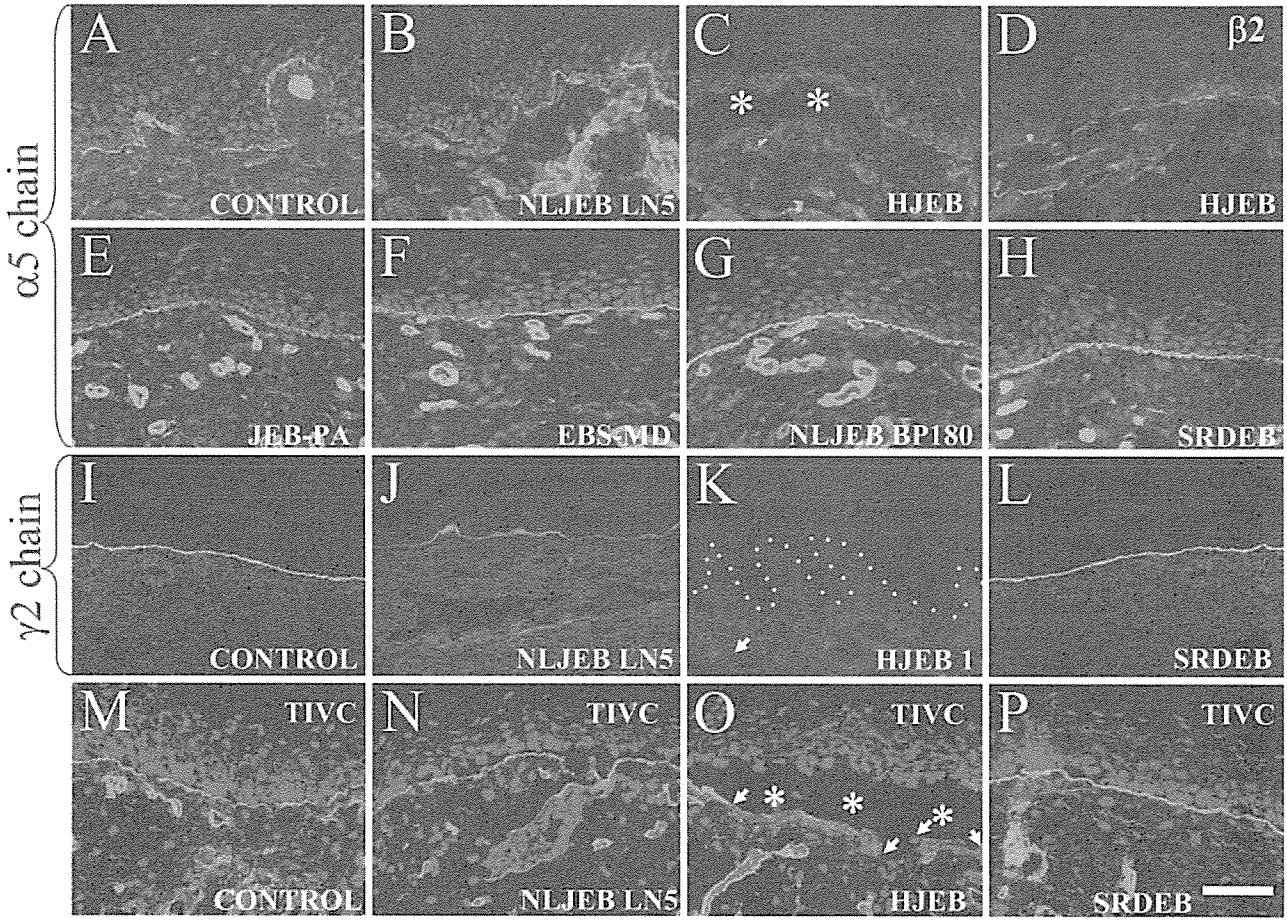

Figure 4 Laminin α5 and β2 chains are expressed beneath the epidermis in epidermolysis bullosa (EB) skin but are focally reduced in split lethal Herlitz junctional EB (HJEB) skin. The laminin α5 chain in control skin showed linear fluorescence along the dermal–epidermal junction and in dermal blood vessels (**A**). However, in non-lethal (**B**) and HJEB skin (**C,D**), the laminin α5 and β2 chains showed reductions in dermal–epidermal junction staining, especially where areas of skin had become separated (**C**, asterisks). This effect was due to antigen degradation in HJEB skin during skin separation as demonstrated by reduced collagen IV staining (**O**, arrows:) over the split areas (**O**, asterisks), whereas control skin (**M**), non-lethal junctional EB (NLJEB) (**N**) and dystrophic EB skin (**P**) showed bright linear collagen IV staining, respectively. The presence of α5 and β2 chain staining in intact EB skin demonstrates that these chains are independently synthesized and maintained even in the presence of other defective basement membrane components. All other cases of EB showed normal staining for the laminin α5 chain (and β2 chain, not shown), including junctional EB associated with pyloric atresia (JEB-PA with defects in α6β4 integrin (**E**), EB simplex associated with muscular dystrophy (EBS-MD with defects in plectin) (**F**), NLJEBBP180 with defects in BP180 (**G**), and severe recessive dystrophic EB (SRDEB with collagen VII defects (**H**). In control and SRDEB patients' skin, laminin-5 γ2 chains were normally expressed (**I** and **L**, respectively) using the γ2 chain monoclonal antibody GB3. Laminin-5 expression was severely reduced and absent in both the NLJEB and HJEB cases (**J,K**), respectively, harboring severe defects in laminin 5. Bar = 50 μm.

Figure 5 The majority of laminin 5 and laminin 10/11 chains are restricted to the lamina densa beneath HDs, whereas collagen IV is expressed continuously along the basal lamina. Postembedding immunoelectron microscopy with anti-α5 chain (laminin 10) (**A–D**) and double labeling with anti-α3 chain (laminin 5) (**E**) antibodies in control skin reveals a similar labeling pattern for these laminins. Collagen IV (M3F7), however, is not restricted to beneath HDs but is continuous along the basal lamina (**F**). Double labeling with laminin 5 polyclonal antiserum (15 nm gold particles) and laminin 10/11 (with smaller 5 nm gold particles) shows that the majority of labeling colocalizes beneath HDs at the border between the lamina lucida and lamina densa (**E**). The majority (84%) of laminin α5 chain labeling (see Table 2 and **A–D**) was restricted to areas immediately beneath the HDs, over the LD border (**A–D**, arrows) whereas only 61% of collagen IV was restricted to beneath HDs (**F**). HD plaques (solid arrows) are shown within the keratinocyte cytoplasm (white cross) and the lamina lucida highlighted by asterisks. Bar = 0.2 μm.

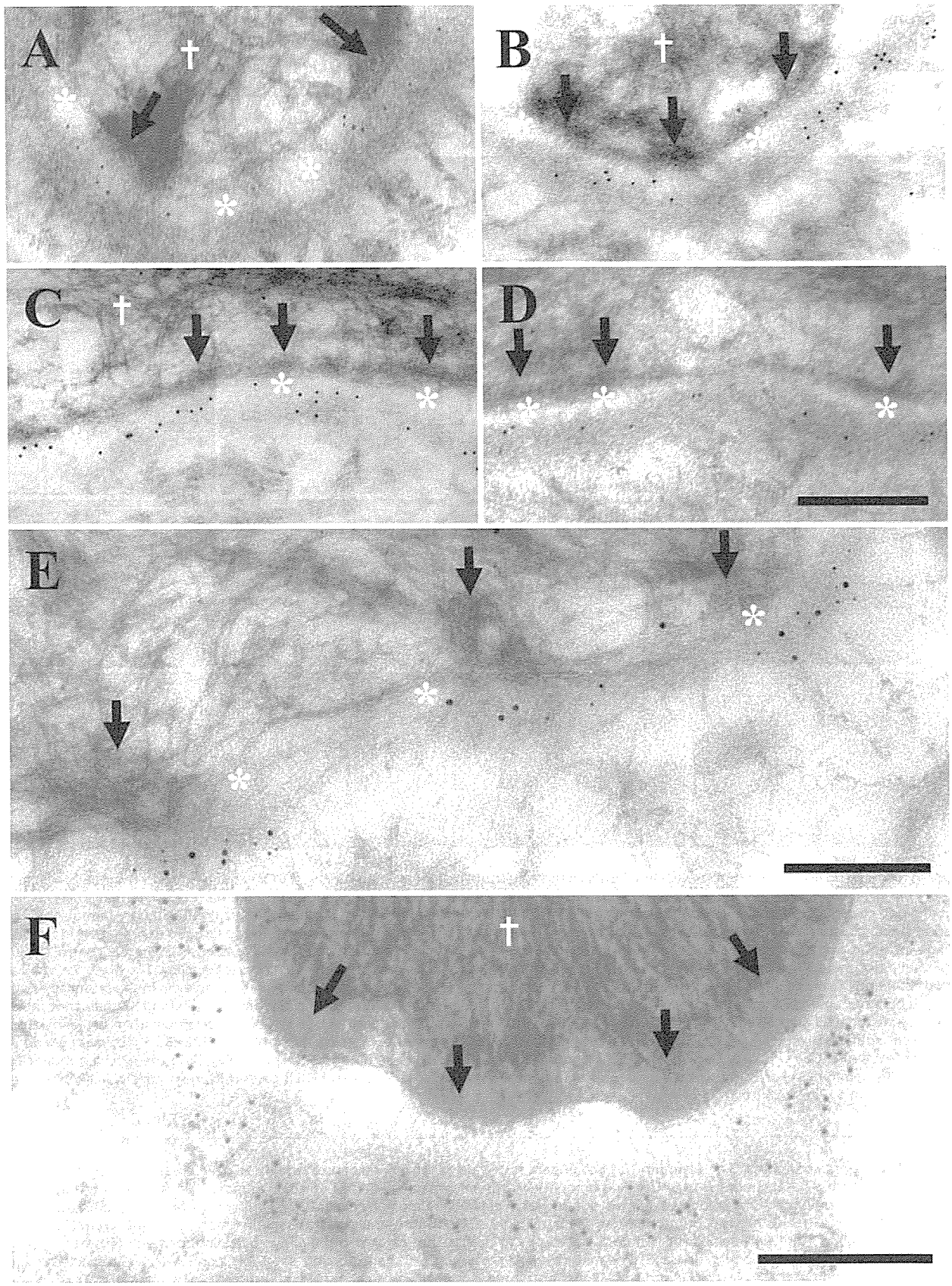

suggested that this effect might be due to antigen degradation in vivo in the split areas. The presence of α5 and β2 chains in intact EB skin, however, confirms that these chains are capable of being independently synthesized and assembled even in the total absence or in the presence of defective laminin 5. All other EB cases also showed normal staining for other laminins including junctional EB associated with pyloric atresia (JEB-PA) (with defects in α6β4 integrin, Figure 4E), EB simplex associated with muscular dystrophy (EBS-MD) (with defects in plectin, Figure 4F), non-lethal junctional (NLJEB) (with defects in BP180, Figure 4G), and severe recessive dystrophic epidermolysis bullosa (SRDEB) (Figure 4H). In control and SRDEB patients' skin there was normal staining for laminin 5 (γ2 chain using the antibody GB3, see Figure 4L). This was in contrast to laminin-5 chain staining that was severely reduced or absent in both the NLJEB (Figure 4J) and HJEB cases (Figure 4K), harboring severe defects in laminin-5 expression.

Immunogold Electron Microscopy and Quantitative Analysis

Labeling of control interfollicular epidermal sections showed that the majority of laminin-10 α5 chains (Figures 5A–5D; Table 2), β1, γ1, and 11 chain (β2 chain, data not shown) were restricted to under the cytoplasmic HD outer plaques. This was in contrast to collagen IV, which was not as restricted to beneath epidermal HDs plaques (see Figure 5F, 61% collagen IV vs 82% laminin 5). The difference between all laminin and collagen values was statistically significant using the one-way ANOVA ($p<0.001$) and Student's *t*-test ($p<0.000$). All four α5, β1, β2, and γ1 chain antibodies and antiserum showed a remarkable similarity in the percentage of labeling associated with the HD attachment plaque and anchoring filament complex beneath HDs, ranging between 84% and 92% (see Table 2). Furthermore, these values reflect an almost identical (HD restricted) expression pattern to the previously reported values for laminin-5 subunits (Masunaga et al. 1996; McMillan et al. 2003b) (part of these findings are also included in Table 2). Our data are very similar to those of laminin 5 (α3 chain) that on average demonstrated 82% of labeling restricted to beneath HDs (see Table 2) at a distance ranging from 35 to 45 nm below the plasma membrane at the LL–LD junction (Masunaga et al. 1996; McMillan et al. 2003b). The precise distance of the 4C7 epitope on the C-terminal portion of the α5 chain was 53.07 nm (±6.69 SD) from the plasma membrane (arrows, Figures 5A–5D). This is 18 nm lower than the G1 domain of the laminin-5 α3 chain described previously (see Figure 1) (McMillan et al. 2003b). The difference between these two α chain mean values was statistically significant using the one-way ANOVA ($p>0.01$) and Student's *t*-test ($p=0.009$). However, visual examination of the distribution of these two antigens revealed overlapping values ~30–40 nm beneath the plasma membrane, the only difference being that the α5 chain showed a wider range of labeling that extended deeper in the LD compared with the α3 chain. The remaining three β1-, β2-, and γ1-chain antibodies recognized, as yet unidentified, epitopes on specific laminin chains and were therefore not included in the plasma membrane distance measurements. However, all three antibodies showed upper LD labeling (not shown), the majority of which were restricted to beneath HDs similar to the α5 chain. The three β1-, β2-, and γ1-chain antibodies were excluded from the distance measurements but were scored for their localization either beneath visible HD attachment plaques (as defined by McMillan and Eady 1996) or within inter-HD areas.

Double labeling for the α5 chain of laminins 10/11 (highlighted by 5-nm small gold particles) and whole anti-laminin 5 antiserum (shown by the larger 15-nm gold particles) shows a similar labeling pattern in the LD beneath electron densities presumed to be HDs (Figure 5E). HD plaques are visible within the keratinocyte cytoplasm (white cross) and the dermal–epidermal junction is separated by the LL (Figure 5E, asterisks). Together our data suggest that the α5 chains (including β1, β2, and γ1 chains, see Table 2) show a restricted expression pattern beneath HDs, similar to laminin 5 but unlike collagen IV.

Discussion

We have demonstrated that the α5, β1, and γ1 chains show a similar localization to laminin 5 in the human interfollicular epidermal basement membrane. These data support the presence of multiple laminin isoforms beneath HDs in the basement membrane at several different epidermal sites. A very different localization of collagen IV within the LD but not restricted to beneath HDs was observed. These data suggest a complex network of interactions between different basement membrane components beneath the epidermis (Ghohestani et al. 2001; McMillan et al. 2003a; Miner and Yurchenco 2004).

In addition we have demonstrated that the expression of the α5 and β2 chains is independent of laminin 5, as demonstrated by residual staining in HJEB patients' skin. The reduction in α5 and β2 chain expression in HJEB was only observed over separated, blistered areas of skin, suggesting that this effect is due to separation-induced antigen degradation in vivo. This was supported by reduced collagen IV staining in split areas of EB skin. This was confirmed after reduced collagen IV staining was observed within separated areas of HJEB skin samples (data not shown). Our

results also suggest that the presence of other laminins cannot fully compensate for defects in laminin-5-deficient HJEB skin (McMillan et al. 1997,1998). The α5 and β2 chains were also normally expressed in all other EB samples harboring defects in plectin, collagen XVII (bullous pemphigoid antigen 2), the α6β4 integrin, and collagen VII.

In previous reports (Aumailley and Rousselle 1999), the laminin β2 chain was not expressed in the epidermal basement membrane of neonatal foreskin. However, we showed weak, variable β2 chain expression (in thigh and arm skin) and absences in other body sites (scalp skin). We conclude that the lack of β2 staining may be due to several factors: antigen masking, a low-level expression, or site- or age-specific variations in human laminin β2 chain expression that may include posttranslational protein processing seen in other laminin isoforms (Miner et al. 1997).

Laminin 5, together with several HD-associated antigens, is expressed in a specific pattern around late anagen hair follicles that excludes staining around the dermal papilla area (Akiyama et al. 1995; Nutbrown and Randall 1995). Laminin-10 chains also show this similar expression pattern in late anagen hair follicles. Unlike laminin-5 and laminin-10 chains, we failed to observe any β2 chain expression (laminins 7/11) in any part of the adult hair follicle; however, this may be due to a low level of antigen expression or masking of the β2 chain epitope. The significance of these findings may be related to the specific growth phases of the lower non-permanent portion of the hair follicle.

In the laminin α5 chain knockout mouse, an unusual disruption in hair follicle morphogenesis was demonstrated (Li, et al., 2003). Li et al. (2003) reported that, in control mice, laminin 10 was present in murine elongating hair germs when other laminins were down-regulated, suggesting a specific role for this laminin in hair follicle development and follicular keratinocyte migration. Mouse skin lacking laminin 10 also contained fewer hair germs and follicles compared with control mice, and after transplantation experiments this skin showed a failure of hair germ elongation and defective basement membrane assembly. Intriguingly, treatment of these mice with purified exogenous laminin 10 corrected these defects and restored hair follicle development. Given that human hair follicles are slow cycling and the majority remains in the late anagen phase and shows different growth characteristics to murine follicles, our failure to demonstrate such growth phase-specific differences in the expression of laminin 10 during the hair cycle stages is not surprising.

The presence of multiple laminin isoforms beneath HDs suggests the hypothesis that there are laminin subunits possibly with overlapping functions that form focal clusters of laminin molecules. This was in contrast to collagen IV, which was not restricted to HDs and localized to the LD region. Ultrastructural data show that the α3 chain (laminin 5) is closer to the plasma membrane than the α5 chain (with only an 18-nm difference, see Table 2). This might suggest that the α5 chain is more closely associated with a LD component such as collagen IV. However, given the size of both laminin chains of ~80–100 nm (as determined by rotary shadowing experiments), our data suggest a significant overlap occurs between α3 and α5 chains (Marinkovich et al. 1992; Vailly et al. 1994). Further studies using a larger battery of antibodies are required to determine the orientation of these laminin components.

Together these data show for the first time that laminin 10/11 chains are restricted to beneath HDs similar to laminin 5 but distinct from collagen IV. Our data suggest a specific localization of multiple laminin isoforms in the epidermal basement membrane beneath HDs and support the hypothesis that several laminins in close association may promote stable cell attachment among different basement membrane molecules.

Acknowledgments

This work was supported by a grant-in-aid of Scientific Research A (13357008, HS) and Health and Labor Sciences Research Grants (Research into Specific Diseases) H13-Saisei-02 and H17-Saisei 12, by a grant from the Japanese Society for the Promotion of Science (JSPS) grant #00345 to J.R.M., and by a grant-in-aid for JSPS fellows' research expenses (#00345). This work was also supported by a grant from the Japanese Health Science Foundation for Research Residents, for class "A" researchers (JRM).

We gratefully acknowledge the technical support of Ms. M. Sato and Ms. K. Sakai in this study. We also thank Dr. T. Masunaga for kindly providing the data from the γ2 chain study (Masunaga et al. 1996) and Dr. M.P. Marinkovich for his kind gift of his polyclonal laminin 5 antibody. Hybridoma supernatants D18 and 2E8 (produced by Drs. J. Sanes and E. Engvall) and M3F7 (from Dr. H. Furthmeyer) were obtained from the Developmental Studies Hybridoma Bank, developed under the auspices of the National Institute of Child Health and Human Development (NICHD) and maintained by the University of Iowa, Department of Biological Sciences, Iowa City, Iowa.

Literature Cited

Akiyama M, Dale BA, Sun TT, Holbrook KA (1995) Characterization of hair follicle bulge in human fetal skin: the human fetal bulge is a pool of undifferentiated keratinocytes. J Invest Dermatol 105: 844–850

Aumailley M, Rousselle P (1999) Laminins of the dermo-epidermal junction. Matrix Biol 18:19–28

Engvall E, Davis GE, Dickerson K, Ruoslahti E, Varon S, Manthorpe M (1986) Mapping of domains in human laminin using monoclonal antibodies: localization of the neurite-promoting site. J Cell Biol 103:2457–2465

Engvall E, Earwicker D, Haaparanta T, Ruoslahti E, Sanes JR (1990) Distribution and isolation of four laminin variants; tissue restricted distribution of heterotrimers assembled from five different subunits. Cell Regul 1:731–740

Foellmer HG, Madri JA, Furthmayr H (1983) Methods in laboratory investigation. Monoclonal antibodies to type IV collagen: probes

for the study of structure and function of basement membranes. Lab Invest 48:639–649
Geuijen CA, Sonnenberg A (2002) Dynamics of the α6β4 integrin in keratinocytes. Mol Biol Cell 13:3845–3858
Ghohestani RF, Li K, Rousselle P, Uitto J (2001) Molecular organization of the cutaneous basement membrane zone. Clin Dermatol 19:551–562
Gu J, Sumida Y, Sanzen N, Sekiguchi K (2001) Laminin-10/11 and fibronectin differentially regulate integrin-dependent Rho and Rac activation via p130(Cas)-CrkII-DOCK180 pathway. J Biol Chem 276:27090–27097
Hunter DD, Shah V, Merlie JP, Sanes JR (1989) A laminin-like adhesive protein concentrated in the synaptic cleft of the neuromuscular junction. Nature 338:229–234
Kennedy AR, Heagerty AH, Ortonne JP, Hsi BL, Yeh CJ, Eady RA (1985) Abnormal binding of an anti-amnion antibody to epidermal basement membrane provides a novel diagnostic probe for junctional epidermolysis bullosa. Br J Dermatol 113:651–659
Kikkawa Y, Sanzen N, Fujiwara H, Sonnenberg A, Sekiguchi K (2000) Integrin binding specificity of laminin-10/11: laminin-10/11 are recognized by α3β1, α6β1 and α6β4 integrins. J Cell Sci 113:869–876
Kikkawa Y, Sanzen N, Sekiguchi K (1998) Isolation and characterization of laminin-10/11 secreted by human lung carcinoma cells. Laminin-10/11 mediates cell adhesion through integrin α3β1. J Biol Chem 273:15854–15859
Li J, Tzu J, Chen Y, Zhang YP, Nguyen NT, Gao J, Bradley M, et al. (2003) Laminin-10 is crucial for hair morphogenesis. EMBO J 22: 2400–2410
Makino M, Okazaki I, Kasai S, Nishi N, Bougaeva M, Weeks BS, Otaka A, et al. (2002) Identification of cell binding sites in the laminin α5-chain G domain. Exp Cell Res 277:95–106
Marinkovich MP, Lunstrum GP, Burgeson RE (1992) The anchoring filament protein kalinin is synthesized and secreted as a high molecular weight precursor. J Biol Chem 267:17900–17906
Masunaga T, Shimizu H, Ishiko A, Tomita Y, Aberdam D, Ortonne JP, Nishikawa T (1996) Localization of laminin-5 in the epidermal basement membrane. J Histochem Cytochem 44:1223–1230
McMillan JR, Akiyama M, Shimizu H (2003a) Epidermal basement membrane zone components: ultrastructural distribution and molecular interactions. J Dermatol Sci 31:169–177
McMillan JR, Akiyama M, Shimizu H (2003b) Ultrastructural orientation of laminin 5 in the epidermal basement membrane: an updated model for basement membrane organization. J Histochem Cytochem 51:1299–1306
McMillan JR, Eady RA (1996) Hemidesmosome ontogeny in digit skin of the human fetus. Arch Dermatol Res 288:91–97
McMillan JR, McGrath JA, Pulkkinen L, Kon A, Burgeson RE, Ortonne J-P, Meneguzzi G, et al. (1997) Immunohistochemical analysis of skin in junctional epidermolysis bullosa using laminin 5 chain specific antibodies is of limited value in predicting the underlying gene mutation. Br J Dermatol 136:817–822
McMillan JR, McGrath JA, Tidman MJ, Eady RA (1998) Hemidesmosomes show abnormal association with the keratin filament network in junctional forms of epidermolysis bullosa. J Invest Dermatol 110:132–137
Mercurio AM, Rabinovitz I, Shaw LM (2001) The α6β4 integrin and epithelial cell migration. Curr Opin Cell Biol 13:541–545
Miner JH, Patton BL, Lentz SI, Gilbert DJ, Snider WD, Jenkins NA, Copeland NG, et al. (1997) The laminin α chains: expression, developmental transitions, and chromosomal locations of α1–5, identification of heterotrimeric laminins 8–11, and cloning of a novel α3 isoform. J Cell Biol 137:685–701
Miner JH, Yurchenco PD (2004) Laminin functions in tissue morphogenesis. Annu Rev Cell Dev Biol 20:255–284
Niessen CM, Hogervorst F, Jaspars LH, de Melker AA, Delwel GO, Hulsman EH, Kuikman I, et al. (1994) The α6β4 integrin is a receptor for both laminin and kalinin. Exp Cell Res 211:360–367
Nishiyama T, Amano S, Tsunenaga M, Kadoya K, Takeda A, Adachi E, Burgeson RE (2000) The importance of laminin 5 in the dermal-epidermal basement membrane. J Dermatol Sci 24(suppl 1): S51–59
Nutbrown M, Randall VA (1995) Differences between connective tissue-epithelial junctions in human skin and the anagen hair follicle. J Invest Dermatol 104:90–94
Pouliot N, Saunders NA, Kaur P (2002) Laminin 10/11: an alternative adhesive ligand for epidermal keratinocytes with a functional role in promoting proliferation and migration. Exp Dermatol 11: 387–397
Pulkkinen L, Smith FJ, Shimizu H, Murata S, Yaoita H, Hachisuka H, Nishikawa T, et al. (1996) Homozygous deletion mutations in the plectin gene (PLEC1) in patients with epidermolysis bullosa simplex associated with late-onset muscular dystrophy. Hum Mol Genet 5:1539–1546
Sanes JR, Engvall E, Butkowski R, Hunter DD (1990) Molecular heterogeneity of basal laminae: isoforms of laminin and collagen IV at the neuromuscular junction and elsewhere. J Cell Biol 111: 1685–1699
Shimizu H, McDonald JN, Gunner DB, Black MM, Bhogal B, Leigh IM, Whitehead PC, et al. (1990) Epidermolysis bullosa acquisita antigen and the carboxy terminus of type VII collagen have a common immunolocalization to anchoring fibrils and lamina densa of basement membrane. Br J Dermatol 122:577–585
Shimizu H, McDonald JN, Kennedy AR, Eady RAJ (1989) Demonstration of intra- and extra-cellular localization of bullous pemphigoid antigen using cryofixation and freeze substitution for postembedding immuno-electron microscopy. Arch Dermatol Res 281:443–448
Takizawa Y, Pulkkinen L, Shimizu H, Lin L, Hagiwara S, Nishikawa T, Uitto J (1998a) Maternal uniparental meroisodisomy in the LAMB3 region of chromosome 1 results in lethal junctional epidermolysis bullosa. J Invest Dermatol 110:828–831
Takizawa Y, Shimizu H, Pulkkinen L, Hiraoka Y, McGrath JA, Suzumori K, Aiso S, et al. (1998b) Novel mutations in the LAMB3 gene shared by two Japanese unrelated families with Herlitz junctional epidermolysis bullosa, and their application for prenatal testing. J Invest Dermatol 110:174–178
Takizawa Y, Shimizu H, Pulkkinen L, Nonaka S, Kubo T, Kado Y, Nishikawa T, et al. (1998c) Novel premature termination codon mutations in the laminin γ2-chain gene (LAMC2) in Herlitz junctional epidermolysis bullosa. J Invest Dermatol 111:1233–1234
Takizawa Y, Shimizu H, Pulkkinen L, Suzumori K, Kakinuma H, Uitto J, Nishikawa T (1998d) Combination of a novel frameshift mutation (1929delCA) and a recurrent nonsense mutation (W610X) of the LAMB3 gene in a Japanese patient with Herlitz junctional epidermolysis bullosa, and their application for prenatal testing. J Invest Dermatol 111:1239–1241
Tiger CF, Champliaud MF, Pedrosa-Domellof F, Thornell LE, Ekblom P, Gullberg D (1997) Presence of laminin α5 chain and lack of laminin α1 chain during human muscle development and in muscular dystrophies. J Biol Chem 272:28590–28595
Uitto J, Pulkkinen L (2001) Molecular genetics of heritable blistering disorders. Arch Dermatol 137:1458–1461
Vailly J, Verrando P, Champliaud MF, Gerecke D, Wagman DW, Baudoin C, Aberdam D, et al. (1994) The 100-kDa chain of nicein/kalinin is a laminin B2 chain variant. Eur J Biochem 219: 209–218
Yu H, Talts JF (2003) β1 Integrin and α-dystroglycan binding sites are localized to different laminin-G-domain-like (LG) modules within the laminin α5 chain G domain. Biochem J 371:289–299

Microbiology (2006), 152, 2951–2958 DOI 10.1099/mic.0.29100-0

The role of the histidine-35 residue in the cytocidal action of HM-1 killer toxin

Masahiko Miyamoto,[1] Naohiko Onozato,[1] Dakshnamurthy Selvakumar,[1] Tetsuya Kimura,[2] Yasuhiro Furuichi[3] and Tadazumi Komiyama[1]

Correspondence
Masahiko Miyamoto
miyamoto@niigata-pharm.ac.jp

[1]Department of Biochemistry, Faculty of Pharmaceutical Sciences, Niigata University of Pharmacy and Applied Life Sciences, 265-1 Higashizima, Niigata 956-8603, Japan

[2]Faculty of Bioresources, Mie University, Tsu, Mie 514-8507, Japan

[3]GeneCare Research Institute Co. Ltd, Kamakura 247-0063, Japan

Diethylpyrocarbonate modification and site-directed mutagenesis studies of histidine-35 in HM-1 killer toxin (HM-1) have shown that a specific feature, the imidazole side chain of histidine-35, is essential for the expression of the killing activity. In subcellular localization experiments, wild-type HM-1 was in the membrane fraction of *Saccharomyces cerevisiae* BJ1824, but not the HM-1 analogue in which histidine-35 was replaced by alanine (H35A HM-1). Neither wild-type nor H35A HM-1 was detected in cellular fractions of HM-1-resistant yeast *S. cerevisiae* BJ1824 *rhk1*Δ::*URA3* and HM-1-insensitive yeast *Candida albicans* even after 1 h incubation. H35A HM-1 inhibited the activity of partially purified 1,3-β-glucan synthase from *S. cerevisiae* A451, and its extent was almost the same as wild-type HM-1. Co-immunoprecipitation experiments showed that wild-type and H35A HM-1 directly interact with the 1,3-β-glucan synthase complex. These results strongly suggest that histidine-35 has an important role in the cytocidal action of HM-1 that participates in the binding process to the HM-1 receptor protein on the cell membrane, but it is not essential for the interaction with, and inhibition of, 1,3-β-glucan synthase.

Received 28 April 2006
Revised 13 July 2006
Accepted 20 July 2006

INTRODUCTION

HM-1 killer toxin (HM-1) is a strong anti-yeast protein produced by the yeast *Williopsis saturnus* var. *mrakii* IFO 0895 and belongs to the K9-type killer toxin group (Young & Yagiu, 1978; Kimura *et al.*, 1995). HM-1 kills susceptible yeasts effectively, consists of 88 amino acids, including five disulfide cross-links, and is very stable against heat treatment and at pH 2–11 (Yamamoto *et al.*, 1986; Komiyama *et al.*, 1996).

Some killer toxins bind to the yeast cell wall as the first receptor (Bussey *et al.*, 1979; Hutchens & Bussey, 1983; Tipper & Schmitt, 1991; Marquina *et al.*, 2002). HM-1 is believed to bind in this way, then bind to a putative receptor on the cell membrane and finally inhibit 1,3-β-glucan synthase (Kasahara *et al.*, 1994; Takasuka *et al.*, 1995; Kimura *et al.*, 1998).

Previously, by using an alanine-scanning method, we showed that several amino acid residues in HM-1 are required for the expression of killing activity (Miyamoto *et al.*, 2005). In particular, replacement of histidine-35, which is the only histidine residue in the HM-1 molecule, caused a loss of HM-1 killing activity, but it did not affect strongly its secretion efficiency. In this study, to examine the importance of specific features of histidine-35 in the killing activity, we replaced histidine-35 with other amino acids by using site-directed mutagenesis, and measured the amounts of HM-1 secreted and killing activities. To clarify the importance of histidine-35 in the binding process to yeast cells, we examined subcellular localization of wild-type HM-1 and H35A HM-1 in yeast whole cells and spheroplasts. We also determined the mode of action of the 1,3-β-glucan synthase inhibition and the interaction with the 1,3-β-glucan synthase complex by wild-type HM-1 and H35A HM-1. The results showed that histidine-35 is required for the binding of HM-1 to the sensitive yeast receptor in the membrane fraction and this also involves the Rhk1 protein.

Abbreviations: CD, circular dichroism; DEPC, diethylpyrocarbonate; HM-1, HM-1 killer toxin.

METHODS

Materials. HM-1, the HM-1 gene, plasmid YEp51, the HM-1-resistant strain of *Saccharomyces cerevisiae* BJ1824 *rhk1*Δ::*URA3* and other strains, including *Candida albicans*, were obtained as reported previously (Kimura *et al.*, 1993; Komiyama *et al.*, 1996). Anti-1,3-β-glucan synthase catalytic subunit (Fks1p) mouse monoclonal antibody 1F4 was a kind gift from Dr. Watanabe of Japan Roche Research Institute (Kamakura, Japan). Anti-aldehyde dehydrogenase (Ald4p) rabbit polyclonal antibody was prepared by Nordic Immunological Laboratories. The YPD medium consisted of 1% yeast extract, 2% peptone and 2% glucose. Rabbit polyclonal and

mouse monoclonal antibodies against HM-1 were prepared by Nippon Bio-Test Laboratories. An LA PCR *in vitro* mutagenesis kit was obtained from Takara Shuzo (Shirai *et al.*, 2000), and the oligonucleotide primers used were: 5′-TAACCATCCAAGCGACATTAGCT-3′ for H35A HM-1 toxin and 5′-TAACCATCCANNNNACATTAGCT-3′ for H35X HM-1 toxin, where N is one of the 4 nucleotides and X is one of the 20 amino acids.

General methods. Recombinant DNA methods were carried out according to Sambrook *et al.* (1989). The DNA was sequenced by using the dideoxy method with fluorochrome-labelled dNTPs and a Long Read tower DNA sequencer (Amersham Pharmacia Biotech). 3D structures of HM-1 were analysed from the NMR data (Antuch *et al.*, 1996). HM-1 and its analogues were quantified by using ELISA with the purified HM-1 and rabbit polyclonal or mouse monoclonal antibodies (Komiyama *et al.*, 2004).

Chemical modification of histidine residue. HM-1 was reacted with 5 mM diethylpyrocarbonate (DEPC) in PBS at pH 7·4 [PBS (−)] at 20 °C for 30 min, and then excess DEPC was quenched with 20 mM histidine (Miles, 1977). The amount of modified residue was calculated as the increase in the absorbance at 240 nm ($\varepsilon = 3200\ M^{-1}\ cm^{-1}$).

Mutant HM-1 gene construction and expression. Construction of mutant HM-1 genes and the expression of mutant HM-1 analogues were carried out as reported previously (Shirai *et al.*, 2000). The mutant gene-containing plasmids were used to transform HM-1-resistant *S. cerevisiae* BJ1824 *rhk1*Δ::*URA3*. Amino acid replacement at histidine-35 was confirmed by nucleotide sequencing after transformation. Yeasts bearing the genes for HM-1 and its analogues were grown for 48 h at 30 °C in liquid medium consisting of 1 % yeast extract, 2 % peptone, 2 % galactose, 0·5 % sucrose (YPGal + suc). After cultivation, the supernatant was collected by centrifugation, passed through a cellulose acetate filter (pore size 0·45 μm), and then dialysed against deionized distilled water for 16 h at 4 °C. The dialysates were concentrated using an evaporator and then were kept at 4 °C.

SDS-PAGE and Western blotting. SDS-PAGE and immunoblotting were carried out as reported previously (Tsang *et al.*, 1983; Schäger & von Jagow, 1987). The HM-1 and its analogues were detected using anti-HM-1 rabbit polyclonal antibody as the primary antibody and horseradish peroxidase- or alkaline phosphatase-conjugated anti-rabbit IgG as the secondary antibody. Fks1p was detected using anti-Fks1p mouse monoclonal antibody 1F4 as the primary antibody and alkaline phosphatase-conjugated anti-mouse IgG as the secondary antibody. As detection dyes, 3-amino-9-ethylcarbazole for horseradish peroxidase and Western Blue stabilized substrate for alkaline phosphatase (Promega) were used.

Circular dichroism (CD) spectrum. The far-UV CD spectra of HM-1 were measured between 190 and 260 nm by using a JASCO J-820 spectropolarimeter at 25 °C. Sample solutions consisted of 10 μM wild-type or H35A HM-1 and PBS (−).

Measurement of killing activity of HM-1. The killer eclipse assay was used as described by Kishida *et al.* (1996), using *Hansenula anomala* IFO 0569 as test strain. This yeast (3 μl) at 1×10^6 cells ml^{-1} was spotted onto agar plates consisting of YPGal + suc, mutant HM-1 gene-bearing yeasts were planted on the edges of the test strain spots, and then the spots were incubated for 24 h at 30 °C. To estimate killing activities and IC_{50} values (the concentration required for 50 % inhibition of the growth) test yeast *S. cerevisiae* A451 cells at exponential phase were incubated for 12 h in YPD medium with various concentrations of HM-1 or its analogues at 30 °C with reciprocal shaking at 120 r.p.m. The optical densities of the culture broths were then measured at 600 nm using a spectrophotometer, and the IC_{50} values were read from the semi-logarithmic graphs (Komiyama *et al.*, 1996).

Subcellular localization of HM-1. HM-1 localization in yeast cells was determined as described by Suzuki *et al.* (2001). Exponentially growing *S. cerevisiae* and *C. albicans* yeast cells (3×10^7 cells ml^{-1}) were collected by centrifugation at 6000 r.p.m. for 3 min at 25 °C and washed with 0·5 ml water, then suspended in 250 μl 50 mM phosphate buffer pH 6·0 containing 1·2 M sorbitol with or without wild-type HM-1 or H35A HM-1 (10 μg ml^{-1}). The mixtures were incubated at 30 °C for 1 h and were centrifuged at 3000 r.p.m. for 3 min at 4 °C. The supernatant became the 'unbound' fraction. The collected cells were washed five times with 0·5 ml 50 mM phosphate buffer pH 6·0 containing 1·2 M sorbitol. The washed cells were suspended in 0·1 M sodium carbonate pH 11 containing 1·2 M sorbitol and kept on ice for 30 min to extract cellular components that weakly bind on the surface of plasma membrane. The cells were collected by centrifugation at 3000 r.p.m. for 3 min at 4 °C and the supernatant became the 'periplasmic fraction'. The collected cells were suspended in 50 mM Tris/HCl pH 7·5 containing 1 mM EDTA, 1 μM PMSF, 1 μg leupeptin ml^{-1} and 1 μg pepstatin A ml^{-1}, and vortexed with glass beads. The mixture was centrifuged at 1000 *g* for 5 min at 4 °C and the pellet was collected as the 'cell wall fraction'. The supernatant was centrifuged at 100 000 *g* for 30 min at 4 °C, and the pellet was collected as the 'membrane fraction' and the supernatant as the 'cytosolic fraction'. Each fraction was subjected to SDS-PAGE and Western blotting. Completion of each cellular fractionation was determined by Western blotting using anti-Fks1p mouse monoclonal antibody 1F4 for the membrane fraction and anti-aldehyde dehydrogenase Ald4p rabbit polyclonal antibody for the cytosolic fraction. Spheroplasts were prepared using Zymolyase 100T, as described previously (Komiyama *et al.*, 2002).

Partial purification of 1,3-β-glucan synthase. Partial purification of 1,3-β-glucan synthase used the method described previously (Takasuka *et al.*, 1995). Briefly, exponentially growing *S. cerevisiae* A451 cells (3×10^7 cells ml^{-1}) were collected by centrifugation and were disrupted with glass beads in 50 mM Tris/HCl pH 7·5 containing 10 mM EDTA, 0·5 M NaCl, 1 μM PMSF, 1 μg leupeptin ml^{-1} and 1 μg pepstatin A ml^{-1}, and centrifuged at 1000 *g* for 5 min at 4 °C. The supernatant was centrifuged at 100 000 *g* for 30 min at 4 °C. The precipitate was suspended in buffer A (50 mM Tris/HCl pH 7·5, 1 mM EDTA, 1 mM 2-mercaptoethanol, 33 % glycerol) containing 0·16 M NaCl, 20 μM guanosine 5′-[γ-thio]triphosphate (GTPγS), 5 mM DTT, 0·5 % CHAPS and 0·1 % cholesteryl hemisuccinate (CHS), and was incubated for 30 min at 4 °C. The suspension was centrifuged at 100 000 *g* for 30 min at 4 °C, and then 20 mM KF and 5 mM uridine diphosphate glucose (UDP-Glc) were added to the supernatant, and the mixture was incubated for 30 min at 30 °C. 1,3-β-Glucan polymer was formed and was collected by centrifugation at 1500 *g* for 5 min at 4 °C. The pellet was washed twice with buffer B (buffer A, 4 μM GTPγS, 1 mM DTT, 0·4 % CHAPS and 0·08 % CHS) and 10 mM UDP-Glc. 1,3-β-Glucan synthase was extracted from the pellet by incubation with buffer B for 10 min at 30 °C.

Measurement of 1,3-β-glucan synthase activity. 1,3-β-Glucan synthase activities were examined as described previously (Takasuka *et al.*, 1995). Briefly, 2 μl partially purified 1,3-β-glucan synthase was incubated in 40 μl reaction mixture consisting of 20 mM Tris/HCl pH 7·5, 0·4 mM EDTA, 20 mM KF and 5 mM UDP-Glc containing 0·02 kBq UDP-[U-^{14}C]glucose for 60 min at 30 °C. After incubation, 250 μl cold 10 % trichloroacetic acid was added. The solution was kept at 4 °C for 10 min and then was filtered through glass. The filters were washed four times with cold 10 % trichloroacetic acid and then twice with 95 % ethanol. The radioactivities retained on

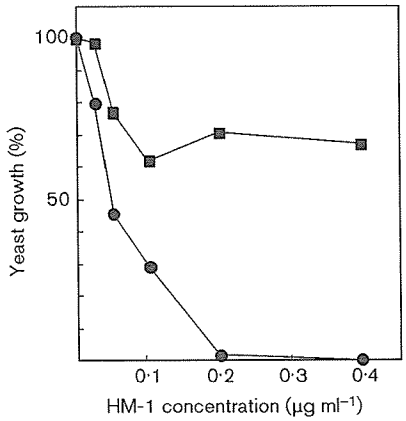

Fig. 1. Yeast killing activity of HM-1 and DEPC-modified HM-1 against *S. cerevisiae* A451. Procedures for the modification of HM-1 with DEPC and killing activity measurement are described in Methods. ●, wild-type HM-1; ■, DEPC-modified HM-1.

the filter were counted using a liquid scintillation counter. To measure the inhibition of 1,3-β-glucan synthase, wild-type or H35A HM-1 was added to the reaction mixture at various concentrations. The reactions were done in triplicate.

Co-immunoprecipitation of HM-1 and 1,3-β-glucan synthase. Co-immunoprecipitation was carried out as described by Harlow & Lane (1999). After mixing 0·6 μg partially purified 1,3-β-glucan synthase with 20 ng wild-type HM-1 or H35A HM-1, 1 μl anti-HM-1 rabbit serum or 0·5 μl anti-Fks1p mouse monoclonal antibody 1F4 was added. BSA (0·6 μg) was used in place of HM-1 and 1,3-β-glucan synthase as the negative control. Then the solution was combined with 10 μl protein G-Sepharose 4 Fast Flow (Amersham Pharmacia) and kept on ice for 1 h with occasional mixing. The mixture was then centrifuged and the precipitate washed four times with PBS (−) containing 0·1 % CHAPS and 0·02 % CHS. The precipitate was incubated with SDS-PAGE sample buffer at 96 °C for 5 min and the supernatant subjected to SDS-PAGE and Western blotting.

RESULTS

Modification of HM-1 with DEPC

In our previous study (Miyamoto *et al.*, 2005), the importance of histidine-35 in HM-1 for the expression of yeast killing activity was shown by using site-directed mutagenesis. Therefore, modification of histidine-35 in HM-1 with DEPC was expected to cause loss of the yeast killing activity. After incubation of HM-1 with 5 mM DEPC for 30 min, 1·13 moles of histidine modified for each mole of HM-1 was calculated as an increase in absorbance at 240 nm (Schäger & von Jagow, 1987). Fig. 1 shows the yeast killing activity of wild-type and DEPC-modified HM-1. The strong killing activity of wild-type HM-1 was greatly decreased by DEPC modification, although about 30 % of the killing activity remained. These results indicate that one mole of histidine is essential for the killing activity of HM-1.

SDS-PAGE of HM-1 analogues secreted by mutant gene-bearing yeasts

To verify the importance of the specific characteristic of the imidazole group of histidine-35 in the yeast killing activity by HM-1, we replaced histidine-35 with 19 other amino acids (indicated by their one-letter symbols) using site-directed mutagenesis. Supernatants of the concentrated culture of the HM-1 gene- or histidine-35-substituted HM-1 gene-bearing yeasts were subjected to SDS-PAGE and Western blotting (Fig. 2). All HM-1 analogues, except H35P and H35W HM-1, had 9·5 kDa bands corresponding to the molecular size of wild-type HM-1, but the band intensities varied among the supernatants. These results indicate that HM-1 analogue expressions were successful and the amount of secretion varied among the mutants. H35S and H35T HM-1 showed an extra band that migrated to a higher molecular mass position.

Quantification of secreted HM-1 analogues

Using concentrated culture supernatants, the amounts of HM-1 analogues secreted by mutant gene-bearing yeasts were measured by ELISA (Table 1). H35A, H35K and H35R HM-1 are secreted into the culture broth at about half the amount of wild-type HM-1. The amounts of H35M, H35N, H35Q, H35S and H35T HM-1 were about eightfold lower than that of wild-type HM-1, and H35C, H35D, H35E, H35F, H35G, H35I, H35L, H35P, H35V, H35W and H35Y HM-1 were secreted at even smaller amounts.

Estimation of killing activity by killer eclipse assay

To estimate the killing activity of histidine-35-substituted HM-1 analogues against sensitive yeasts, we used a killer eclipse assay (Fig. 3). Test yeast strain, *H. anomala* IFO 0569, had high sensitivity to wild-type HM-1. The wild-type HM-1 gene-bearing yeasts showed strong killing activity

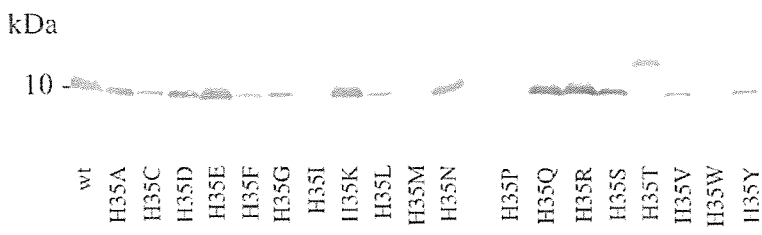

Fig. 2. Western blotting of HM-1 analogues. Aliquots (5 μl) of 20 times concentrated supernatants of cultured broth underwent 15 % SDS-PAGE and then immunoblotting as described in Methods. Amino acids are indicated by one-letter symbols. wt, wild-type.

Table 1. Amounts and IC_{50} values of HM-1 analogues secreted by HM-1 analogue gene-bearing yeasts

Amino acids are indicated by one-letter symbols. ND, Not detected.

Analogue	Concentration (ng ml^{-1})	IC_{50} (ng ml^{-1})
Wild-type	2160	85
H35A	870·0	2575
H35C	7·95	ND
H35D	58·7	ND
H35E	120	ND
H35F	38·9	ND
H35G	67·0	ND
H35I	40·0	ND
H35K	1190	ND
H35L	99·0	ND
H35M	253	ND
H35N	279	ND
H35P	7·10	ND
H35Q	185	ND
H35R	1230	ND
H35S	230	ND
H35T	200	ND
H35V	79·0	ND
H35W	0·45	ND
H35Y	53·1	ND

against *H. anomala*, but all histidine-35-substituted HM-1 gene-bearing yeasts showed no killing activity.

Killing activity estimation by IC_{50} values

Table 1 shows the killing activities of HM-1 analogues measured by IC_{50} values. The IC_{50} value of H35A HM-1 was 30 times larger than for wild-type HM-1. The other histidine-35-substituted HM-1 gene-bearing yeasts showed no killing activity even at the highest concentrations under our experimental conditions. Therefore, we could not estimate the exact IC_{50} values of these HM-1 analogues.

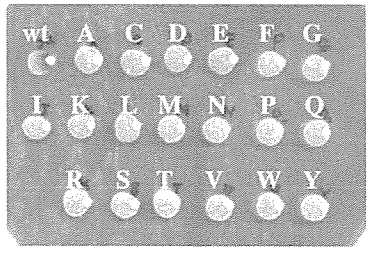

Fig. 3. Killer eclipse assay of HM-1 analogues. *H. anomala* IFO 0569 was used as a test strain. The assay method is described in Methods. wt, wild-type. Substituted amino acids at position 35 in HM-1 are indicated by their one-letter symbol.

CD spectrum of wild-type and H35A HM-1

To examine the possibility that histidine replacement with alanine perturbed the conformation of the secondary structure of HM-1, we carried out a CD spectroscopic analysis of wild-type HM-1 and H35A HM-1. H35A HM-1 had a CD spectrum similar to wild-type HM-1 (Fig. 4), even though H35A HM-1 lost its yeast killing activity.

Subcellular localization of wild-type HM-1 and H35A HM-1

To verify how histidine-35 of HM-1 is related to the location of the protein in yeast cells, we examined subcellular localization of wild-type HM-1 and H35A HM-1, after incubation with yeast cells, using Western blotting. The purity of each subcellular fraction was determined using anti-Fks1p antibody 1F4 for the membrane fraction and anti-aldehyde dehydrogenase Ald4p antibody for the cytosolic fraction. Fig. 5(c) shows that the transmembrane enzyme Fks1p (200 kDa) was detected only in the membrane fraction and cytosolic enzyme Ald4p (56 kDa) was detected in the cytosolic fraction, but some nonspecific bands were also seen in each fraction. Wild-type HM-1 bands were detected in the cell wall fraction and cytosolic fraction of HM-1 sensitive *S. cerevisiae* BJ1824 (lane 1) and *C. albicans* ATCC 10231 (lane 5), and in the membrane fraction of *S. cerevisiae* BJ1824 (lane 1) (Fig. 5a). But H35A HM-1 bands were not detected in any cellular fractions of *S. cerevisiae* and *C. albicans* after 1 h incubation with whole yeast cells (lanes 2, 6). Wild-type and H35A HM-1 bands were not detected in the cellular fractions of *S. cerevisiae* BJ1824 *rhk1*Δ::*URA3* (lanes 3, 4) that is an HM-1-resistant yeast strain (Kimura *et al.*, 1997). In periplasmic fractions, we could not find any band of HM-1 (data no shown). Fig. 5(b) shows the subcellular localizations of wild-type and H35A HM-1 using the spheroplasts. A wild-type HM-1 band was detected in the membrane fraction and weakly in

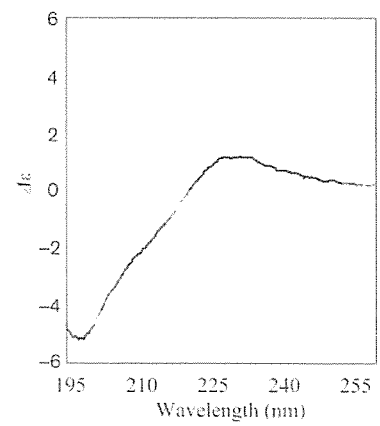

Fig. 4. CD spectra of wild-type and H35A HM-1. Spectra were measured as described in Methods. Black line, wild-type HM-1; grey line, H35A HM-1.

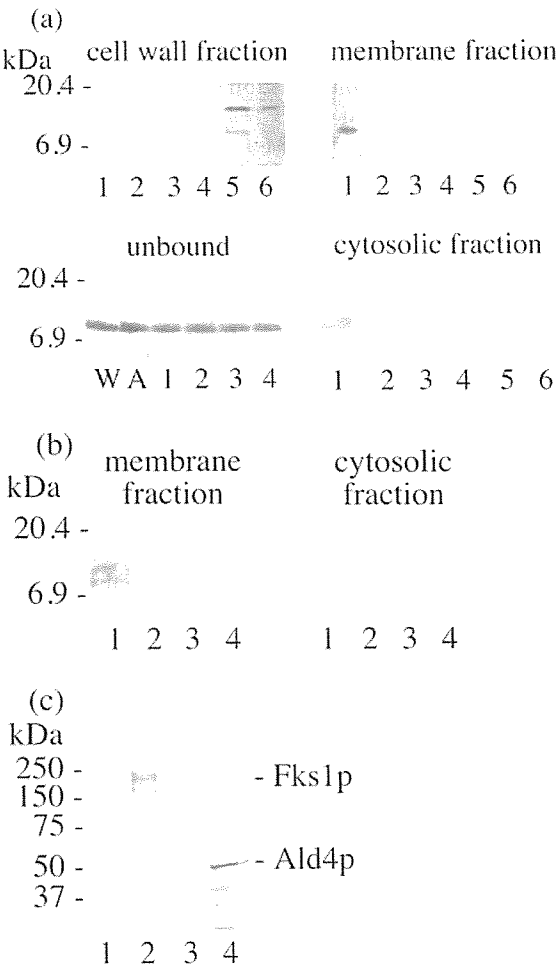

Fig. 5. Subcellular localizations of wild-type HM-1 and H35A HM-1 in *S. cerevisiae* BJ1824 and BJ1824*rhk1*Δ::*URA3*. (a) Yeast whole cells, *S. cerevisiae* BJ1824 (lanes 1, 2), *S. cerevisiae* BJ1824*rhk1*Δ::*URA3* (lanes 3, 4) or *C. albicans* (lanes 5, 6), were incubated with wild-type HM-1 (lanes 1, 3, 5) or H35A HM-1 (lanes 2, 4, 6) and each cell was fractionated as described in Methods. Each fraction was applied to SDS-PAGE and HM-1 bands were detected by Western blotting using anti-HM-1 rabbit serum as the primary antibody. Ten nanograms each of wild-type (W) and H35A (A) HM-1 were electrophoresed as a control. (b) Yeast spheroplasts were used with the same methods as for (a). (c) Completion of each cellular fractionation of *S. cerevisiae* BJ1824 was determined by Western blotting using anti-Fks1p mouse monoclonal antibody 1F4 for the membrane fraction and anti-Ald4p rabbit polyclonal antibody for the cytosolic fraction. Cell wall, membrane, periplasmic and cytosolic fractions of *S. cerevisiae* BJ1824 are shown in lanes 1, 2, 3 and 4, respectively.

the cytosolic fraction of *S. cerevisiae* BJ1824 (lane 1), but the H35A HM-1 band was not detected in the cellular fractions (lane 2). Wild-type and H35A HM-1 bands were not detected in any fractions of *S. cerevisiae* BJ1824 *rhk1*Δ::*URA3* (lane 3, 4). These results show that wild-type HM-1 localizes in the cell membrane whether a cell wall is present or not, but H35A HM-1 does not localize in the cell membrane.

1,3-β-Glucan synthase inhibition by wild-type HM-1 and H35A HM-1

Wild-type HM-1 strongly inhibits 1,3-β-glucan synthase activity of susceptible yeasts (Takasuka *et al.*, 1995). In this study we examined the effect of H35A HM-1 on 1,3-β-glucan synthase activity (Fig. 6). H35A HM-1 inhibited 1,3-β-glucan synthase activity in a concentration dependent manner and at almost the same effectiveness as wild-type HM-1. This result indicates that replacement of histidine-35 with alanine has no effect on the inhibition of 1,3-β-glucan synthase activity by HM-1.

Co-immunoprecipitation of HM-1 and 1,3-β-glucan synthase

We believe that whether or not HM-1 interacts with 1,3-β-glucan synthase directly has not been reported before, and so we carried out a co-immunoprecipitation analysis to verify the direct interaction between HM-1 and 1,3-β-glucan synthase *in vitro* (Fig. 7). Incubations of HM-1 with partially purified 1,3-β-glucan synthase and co-immunoprecipitation with anti-Fks1p antibody were detected using anti-HM-1 rabbit serum as the primary antibody (Fig. 7a). Lane 5 shows that wild-type HM-1 co-immunoprecipitated with 1,3-β-glucan synthase subunit Fks1p, but without Fks1p wild-type HM-1 was not detected (lane 4). By similar incubations H35A HM-1 also co-immunoprecipitated with 1,3-β-glucan synthase, but the intensity of the band was weaker than for wild-type HM-1 (lane 7). These results indicate that wild-type and H35A HM-1 interact with 1,3-β-

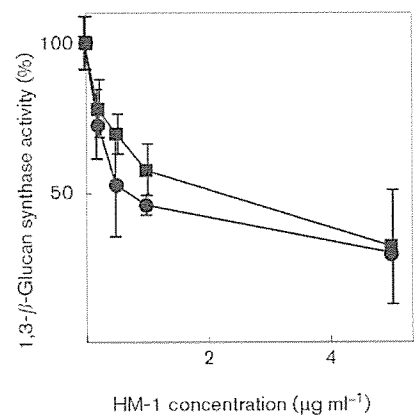

Fig. 6. Inhibition of partially purified 1,3-β-glucan synthase activity by wild-type and H35A HM-1. 1,3-β-Glucan synthase activity was measured in the presence of wild-type HM-1 or H35A HM-1 as described in Methods. ●, wild-type HM-1; ■, H35A HM-1.

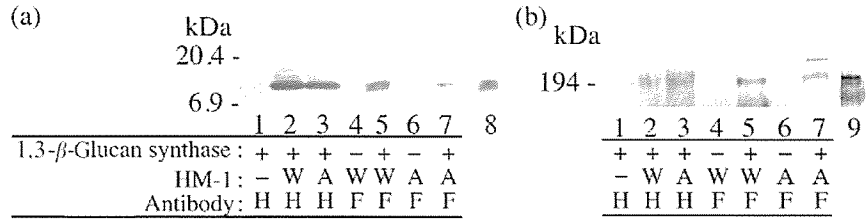

Fig. 7. Co-immunoprecipitation analysis of the interaction between HM-1 and 1,3-β-glucan synthase. After mixing partially purified 1,3-β-glucan synthase (lanes 1, 2, 3, 5, 7) or BSA (lanes 4, 6), with wild-type HM-1 (lanes 2, 4, 5) or H35A HM-1 (lanes 3, 6, 7) or BSA (lane 1), anti-HM-1 rabbit serum (lanes 1–3) or anti-Fks1p mouse monoclonal antibody (lanes 4–7) was added. Protein G-Sepharose 4 Fast Flow was added and centrifuged to precipitate protein molecular complexes. The extracted complexes were subjected to SDS-PAGE and Western blotting using anti-HM-1 rabbit serum (a) or anti-Fks1p mouse monoclonal antibody (b) as the primary antibody for the detection. Wild-type HM-1 (lane 8) and partially purified 1,3-β-glucan synthase (lane 9) were electrophoresed as a control. W, wild-type HM-1; A, H35A HM-1; H, anti-HM-1 rabbit serum; F, anti-Fks1p mouse monoclonal antibody.

glucan synthase directly *in vitro*. In the case of co-immunoprecipitations with anti-HM-1 antibody and detections by anti-Fks1p antibody, the high molecular mass band indicative of Fks1p (molecular mass 200 kDa) precipitated with wild-type and H35A HM-1 (Fig. 7(b), lane 2, 3), but without HM-1, Fks1p was not detected (lane 1). This result also supports our finding that wild-type and H35A HM-1 interact with 1,3-β-glucan synthase *in vitro*.

DISCUSSION

Previously, by using an alanine-scanning method, we showed that histidine-35 is essential for the yeast killing activity of HM-1 (Miyamoto *et al.*, 2005). This conclusion is supported by the DEPC modification experiment of this study (Fig. 1), which modified the sole histidine residue in HM-1 and resulted in the loss of 70 % of the yeast killing activity.

To examine the importance of this histidine residue in HM-1 killing activity, we further substituted histidine-35 by 19 other amino acids, and estimated the amounts of secreted histidine-substituted analogues and their killing activities. All such analogues were successfully expressed and showed bands of the same molecular mass as wild-type HM-1, but in different quantities (Fig. 2). In the case of substitution by hydrophobic amino acid residues, the amounts of HM-1 analogues secreted tended to decrease. In particular, bands of H35P and H35W HM-1 were not found by Western blotting. Probably, in the synthesis process, these amino acid residues destroyed the core structure of HM-1 due to their hydrophobicity or by the steric hindrance of their side chain, and the analogues folded into an unstable structure that was degraded by proteolysis (Kowalski *et al.*, 1998; Ellgaard & Helenius, 2003). H35S and H35T HM-1 had an extra high molecular mass band. Histidine-35 substitution with serine or threonine creates a consensus sequence for the *N*-linked glycosylation site -N-X-S/T- in HM-1, so it is possible that H35S and H35T HM-1 have a glycosylated side chain attachment at the position of aspargine-33. Substitutions by hydrophilic amino acids at the histidine-35 residue yielded varying amounts of HM-1 analogues (Table 1). The amounts of H35A, H35K and H35R HM-1 production were half of wild-type HM-1, but the amounts of other analogues produced were much lower than for wild-type HM-1. These results indicate that position 35 requires a relatively small and/or positively charged amino acid side chain for efficient synthesis and secretion of HM-1.

We estimated the strength of killing activities of HM-1 analogues by killer eclipse assay and IC_{50} measurement. Wild-type HM-1 gene-bearing yeasts had strong killing activity against *H. anomala*, but all histidine-35-substituted HM-1 gene-bearing yeasts showed no killing activity (Fig. 3, Table 1). It is notable that positively charged amino acids lysine and arginine, and aromatic amino acids tyrosine and phenylalanine, did not recover the killing activity. Replacement of histidine-35 with alanine did not affect the secondary structure of HM-1 (Fig. 4). These results indicate that the yeast killing activity of HM-1 requires the specific features of the imidazole group of the histidine side chain at position 35.

Some killer toxins bind to yeast cell wall molecules as a first receptor (Hutchens & Bussey, 1983; Tipper & Schmitt, 1991; Kimura *et al.*, 1998; Marquina *et al.*, 2002).The killing action of *S. cerevisiae* killer toxin K1 is believed to be a multi-step process (Bussey, 1981; Martinac *et al.*, 1990; Kurzweilova & Sigler, 1994; Schmitt & Compain, 1995). The first step is the binding of toxin to the cell wall 1,6-β-glucan, and the next step is interaction with the plasma membrane receptors. The tertiary structure of *Pichia farinosa* killer toxin SMKT is similar to that of HM-1 (Kashiwagi *et al.*, 1997; Kunishima *et al.*, 1997). SMKT localizes on the surface of the plasma membrane and is removed from the membrane by sodium carbonate treatment (Suzuki *et al.*, 2001). HM-1 interacts weakly with the yeast cell wall (Kasahara *et al.*, 1994), but what component interacts with it after this is not clear. Therefore, we examined the subcellular localization of HM-1 in yeasts using whole cells and spheroplasts. Fig. 5(a, b)

(lane 1) shows that wild-type HM-1 localizes in the membrane fraction of HM-1 sensitive yeast cells and spheroplasts. In contrast to SMKT, HM-1 bound strongly to the cell membrane and was not removed by sodium carbonate treatment. However, H35A HM-1 did not localize to the membrane and other fractions in HM-1 sensitive yeast (Fig. 5a, b; lane 2). These results indicate that histidine-35 in HM-1 has an important role in the interaction with molecules of the cell membrane, the putative HM-1 receptors.

C. albicans ATCC 10231 bound to wild-type HM-1 in cell wall and cytosolic fractions, but not in the membrane fraction, and its interactions were weaker than for *S. cerevisiae* BJ1824 (Fig. 5a, lane 5). These may cause the difference in sensitivity of HM-1 against *S. cerevisiae* (MIC = 0·4–1·6 μg ml^{-1}) and *C. albicans* (MIC > 300 μg ml^{-1}) (Yamamoto *et al.*, 1988).

HM-1-resistant yeast *S. cerevisiae* BJ1824 *rhk1Δ::URA3* did not bind to wild-type HM-1 and H35A HM-1 (Fig. 5a, b; lanes 3, 4). The α-1,3-mannosyltransferase Rhk1p participates in the HM-1 sensitivity of yeasts and contributes to the maintenance of the polysaccharide composition of the cell wall and its structure (Kimura *et al.*, 1997, 1999). The HM-1 resistance of *S. cerevisiae* BJ1824 *rhk1Δ::URA3* strain is explained by the deficiency of the Rhk1p causing perturbation of the cell wall structure so that HM-1 cannot bind there. In this study, we showed that wild-type HM-1 interacts with spheroplast membranes, but cannot interact with *RHK1* deleted spheroplast membranes (Fig. 5b). These results indicate that wild-type HM-1 can interact with the putative HM-1 receptor on the cell membrane regardless of whether the cell wall is present or not, and the receptor is likely to need Rhk1p-associated modification in its molecule for interaction with HM-1.

Since a possibility that histidine-35 has an important role in the interaction with 1,3-β-glucan synthase remained, we checked the interaction of HM-1 with 1,3-β-glucan synthase. H35A HM-1 was able to inhibit 1,3-β-glucan synthase to the same extent as wild-type HM-1 (Fig. 6), and H35A HM-1 interacted directly with 1,3-β-glucan synthase *in vitro* (Fig. 7). These results indicate that histidine-35 in HM-1 is not essential for the interaction and inhibition of 1,3-β-glucan synthase. After solubilization of HM-1-treated yeast membrane fraction with various detergents, most HM-1 was not extracted in the same fraction as 1,3-β-glucan synthase (data not shown). These results support the idea that the presence of a putative HM-1 receptor other than 1,3-β-glucan synthase is required on the cell membrane for the interaction with HM-1.

In conclusion, the importance of histidine-35 for the expression of the killing activity of HM-1 was shown by using chemical modification and site-directed mutagenesis. Subcellular localization and co-immunoprecipitation experiments indicated that the role of histidine-35 in HM-1 is related to the binding process of HM-1 to its putative receptor protein, not to the inhibition of 1,3-β-glucan synthase activity.

ACKNOWLEDGEMENTS

This work was supported by a grant from the Ministry of Education, Science, Sports and Culture of Japan.

REFERENCES

Antuch, W., Güntert, P. & Wüthrich, K. (1996). Ancestral β γ-crystallin precursor structure in a yeast killer toxin. *Nat Struct Biol* **3**, 662–665.

Bussey, H. (1981). Physiology of killer factor in yeast. *Adv Microb Physiol* **22**, 93–122.

Bussey, H., Saville, D., Hutchins, K. & Palfree, R. G. E. (1979). Binding of yeast killer toxin to a cell wall receptor on sensitive *Saccharomyces cerevisiae*. *J Bacteriol* **140**, 888–892.

Ellgaard, L. & Helenius, A. (2003). Quality control in the endoplasmic reticulum. *Nat Rev Mol Cell Biol* **4**, 181–191.

Harlow, E. & Lane, D. (1999). *Using Antibodies: a Laboratory Manual.* Cold Spring Harbor, NY: Cold Spring Harbor Laboratory.

Hutchens, K. & Bussey, H. (1983). Cell wall receptor for yeast killer toxin: involvement of (1-6)-β-D-glucan. *J Bacteriol* **154**, 161–169.

Kasahara, S., Inoue, S. B., Mio, T., Yamada, T., Nakajima, T., Ichishima, E., Furuichi, Y. & Yamada, H. (1994). Involvement of cell wall β-glucan in the action of HM-1 killer toxin. *FEBS Lett* **348**, 27–32.

Kashiwagi, T., Kunishima, N., Suzuki, C., Tsuchiya, F., Nikkuni, S., Arata, Y. & Morikawa, K. (1997). The novel acidophilic structure of the killer toxin from halotolerant yeast demonstrates remarkable folding similarity with a fungal killer toxin. *Structure* **5**, 81–94.

Kimura, T., Kitamoto, N., Matsuoka, K., Nakamura, K., Iimura, Y. & Kito, Y. (1993). Isolation and nucleotide sequence of the genes encoding killer toxins from *Hansenula mrakii* and *H. saturnus*. *Gene* **137**, 265–270.

Kimura, T., Kitamoto, N., Kito, Y., Iimura, Y., Shirai, T., Komiyama, T., Furuichi, Y., Sakka, K. & Ohmiya, K. (1997). A novel yeast gene, *RHK1*, is involved in the synthesis of the cell wall receptor for the HM-1 killer toxin that inhibits β-1,3-glucan synthesis. *Mol Gen Genet* **254**, 139–147.

Kimura, T., Iimura, Y., Komiyama, T., Karita, S., Sakka, K. & Ohmiya, K. (1998). Killing mechanism by HM-1 killer toxin of *Hansenula mrakii* and application of HM-1 in fermentation process to prevent contamination with wild yeasts. *Recent Res Dev Ferment Bioeng* **1**, 225–240.

Kimura, T., Kitamoto, N., Ohta, Y., Kito, Y. & Iimura, Y. J. (1995). Structural relationships among killer toxins secreted from the killer strains of the genus *Williopsis*. *J Ferment Bioeng* **80**, 85–87.

Kimura, T., Komiyama, T., Furuichi, Y., Iimura, Y., Karita, S., Sakka, K. & Ohmiya, K. (1999). *N*-glycosylation is involved in the sensitivity of *Saccharomyces cerevisiae* to HM-1 killer toxin secreted from *Hansenula mrakii* IFO 0895. *Appl Microbiol Biotechnol* **51**, 176–184.

Kishida, M., Tokunaga, M., Katayose, Y., Yajima, H., Kawamura-Watabe, A. & Hishinuma, F. (1996). Isolation and genetic characterization of pGKL killer-insensitive mutants (*iki*) from *Saccharomyces cerevisiae*. *Biosci Biotechnol Biochem* **60**, 798–801.

Komiyama, T., Ohta, T., Urakami, H., Shiratori, Y., Takasuka, T., Sato, M., Watanabe, T. & Furuichi, Y. (1996). Pore formation on proliferating yeast *Saccharomyces cerevisiae* cell buds by HM-1 killer toxin. *J Biochem* **119**, 731–736.

Komiyama, T., Kimura, T. & Furuichi, Y. (2002). Round shape enlargement of the yeast spheroplast of *Saccharomyces cerevisiae* by HM-1 toxin. *Biol Pharm Bull* **25**, 959–965.

Komiyama, T., Zhang, Q., Miyamoto, M., Selvakumar, D. & Furuichi, Y. (2004). Monoclonal antibodies and sandwich ELISA for quantitation of HM-1 killer toxin. *Biol Pharm Bull* **27**, 691–693.

Kowalski, J. M., Parekh, R. N., Mao, J. & Wittrup, K. D. (1998). Protein folding stability can determine the efficiency of escape from endoplasmic reticulum quality control. *J Biol Chem* **273**, 19453–19458.

Kunishima, N., Kashigawa, T., Suzuki, C., Tsuchiya, F., Arata, Y. & Morikawa, K. (1997). Crystallization and preliminary X-ray diffraction studies of a novel killer toxin from a halotolerant yeast *Pichia farinosa*. *Acta Crystallogr D Biol Crystallogr* **53**, 112–113.

Kurzweilova, H. & Sigler, K. (1994). Kinetic studies of killer toxin K1 binding to yeast cells indicate two receptor populations. *Arch Microbiol* **162**, 211–214.

Marquina, D., Santos, A. & Peinado, J. M. (2002). Biology of killer yeasts. *Int Microbiol* **5**, 65–71.

Martinac, B., Zhu, H., Kubalski, A. & Zhou, X. (1990). Yeast K1 killer toxin forms ion channels in sensitive yeast spheroplasts and in artificial liposomes. *Proc Natl Acad Sci U S A* **87**, 6228–6232.

Miles, E. W. (1977). Modification of histidyl residues in proteins by diethylpyrocarbonate. *Methods Enzymol* **47**, 431–442.

Miyamoto, M., Han, G.-D., Kimura, T., Furuichi, Y. & Komiyama, T. (2005). Alanine-scanning mutagenesis of HM-1 killer toxin and the essential residues for killing activity. *J Biochem* **137**, 517–522.

Sambrook, J., Fritsh, E. F. & Maniatis, T. (1989). *Molecular Cloning: a Laboratory Manual*, 2nd edn. Cold Spring Harbor, NY: Cold Spring Harbor Laboratory.

Schmitt, M. J. & Compain, P. (1995). Killer-toxin-resistant *kre12* mutants of *Saccharomyces cerevisiae*: genetic and biochemical evidence for a secondary K1 membrane receptor. *Arch Microbiol* **164**, 435–443.

Schäger, H. & von Jagow, G. (1987). Tricine-sodium dodecyl sulfate-polyacrylamide gel electrophoresis for the separation of proteins in the range from 1 to 100 kDa. *Anal Biochem* **166**, 368–379.

Shirai, T., Kimura, T., Furuichi, Y. & Komiyama, T. (2000). The involvement of two specific arginine residues in the action of HM-1 killer toxin was deduced from site-directed mutagenesis. *Biol Pharm Bull* **23**, 998–1000.

Suzuki, C., Ando, Y. & Machida, S. (2001). Interaction of SMKT, a killer toxin produced by *Pichia farinosa*, with the yeast cell membranes. *Yeast* **18**, 1471–1478.

Takasuka, T., Komiyama, T., Furuichi, Y. & Watanabe, T. (1995). Cell wall synthesis specific cytocidal effect of *Hansenula mrakii* toxin-1 on *Saccharomyces cerevisiae*. *Cell Mol Biol Res* **41**, 575–581.

Tipper, D. J. & Schmitt, M. J. (1991). Yeast dsRNA viruses: replication and killer phenotypes. *Mol Microbiol* **5**, 2331–2338.

Tsang, V. C., Peralta, J. M. & Simons, A. R. (1983). Enzyme-linked immunoelectrotransfer blot techniques (EITB) for studying the specificities of antigens and antibodies separated by gel electrophoresis. *Methods Enzymol* **92**, 377–391.

Yamamoto, T., Imai, M., Tachibana, K. & Mayumi, M. (1986). Application of monoclonal antibodies to the isolation and characterization of a killer toxin secreted by *Hansenula mrakii*. *FEBS Lett* **195**, 253–257.

Yamamoto, T., Uchida, K., Hiratani, T., Miyazaki, T., Yagiu, J. & Yamaguchi, H. (1988). *In vitro* activity of the killer toxin from yeast *Hansenula mrakii* against yeasts and molds. *J Antibiot* **41**, 398–403.

Young, T. W. & Yagiu, M. (1978). A comparison of the killer character in different yeasts and its classification. *Antonie van Leeuwenhoek* **44**, 59–77.

Morphology

Coexistence of a systemic lupus erythematosus and porphyria cutanea tarda: case successfully improved by avoidance of sun exposure

Junko Murata, Tadamichi Shimizu, Yasuyuki Tateishi, Riichiro Abe, and Hiroshi Shimizu

From the Department of Dermatology, Hokkaido University Graduate School of Medicine, Kita-ku, Sapporo, Japan

Correspondence
Tadamichi Shimizu
Department of Dermatology
Hokkaido University Graduate School of Medicine
Kita-ku
Sapporo 060–8638
Japan
E-mail: michiki@med.hokudai.ac.jp

Case Report

A 46-year-old Japanese woman presented with vesicles on her nose and the dosal aspect of her hands since 3 months. Physical examination revealed tense blisters and atrophic erythematous plaques on her arms and the dosal side of her hands (Fig. 1a). Erosions were also scattered on the face (Fig. 1b). She also had hypertrichosis on her face. The patient was first diagnosed as having systemic lupus erythematosus (SLE) in 1997 at the age of 41 years, when she presented with alopecia, fever, arthralgia, Raynaud's phenomenon, hemolytic anemia and lymphadenopathy. Liver transaminase levels were slightly elevated. She had no sign of hepatitis including autoimmune hepatitis, drug-related hepatotoxity, alcoholic hepatitis, or viral infection. Systemic lupus erythematosus was well-controlled with a daily 5-mg dose of prednisolone (PSL).

At age of 43 years she developed erythematous plaques with scaling on the back of her hands. Clinically the skin eruptions at that time appeared to be discoid lupus erythematodes. She was treated with a steroid ointment and her eruptions gradually improved, but new skin lesions repeatedly appeared on her hands.

Laboratory investigations at age 46 years while taking PSL 5 mg disclosed the following results: white cell count 3.9×10^9/l with lymphopenia of 0.78×10^9/l, red cell count 3.35×10^{12}/l, hemoglobin of 11.4 g/l, and a platelet count of 165×10^9/l. Liver function profile included total bilirubin was 1.7 mg/dl, GOT 46 IU/l, GPT 82 IU/l, γ-GTP 142 IU/l, and alkaline phosphatase 456 IU/l. Renal function and electrolytes were normal. Antinuclear antibody (ANA) titers were positive at a dilution of 1/80 (normal value, 1/40) with a homogeneous pattern. Histopathological examination of the back of the hands demonstrated a subepidermal blister with slight inflammatory infiltrate. No eosinophilic deposit around the vessels and little edematous change was present in the dermis (Fig. 2). Direct immunofluorescence revealed a granular fashion at the dermoepidermal junction (DEJ) with IgG, IgM, and C_3. Deposition of C_3 around the blood vessels and several clusters of colloid bodies associated with IgM were also observed in the upper dermis. Laboratory value of fractionated porphyrins in her urine revealed the following: uroporphyrin 1080 μg/l (normal: < 20), coproporophrin 110 μg/L (normal < 100), porphobironogen 1.3 mg/l (normal < 2), and δ-aminolevulinic acid 3.5 mg/dl. The value of porphyrins in her serum was within the normal range, confirming the diagnosis of PCT. Subsequently, she was treated with topical steroid ointment, and avoidance of sun exposure was implemented. Three months later the value of uroporphyrin and coproporphirin in her urine was almost normal and no further blisters appeared.

Discussion

Since the association of SLE and PCT was first described by Linden in 1954,[1] approximately 50 cases of LE (all variants) have been described in association with PCT, including 15 cases reported by Gibson and McEvoy.[2] PCT results from

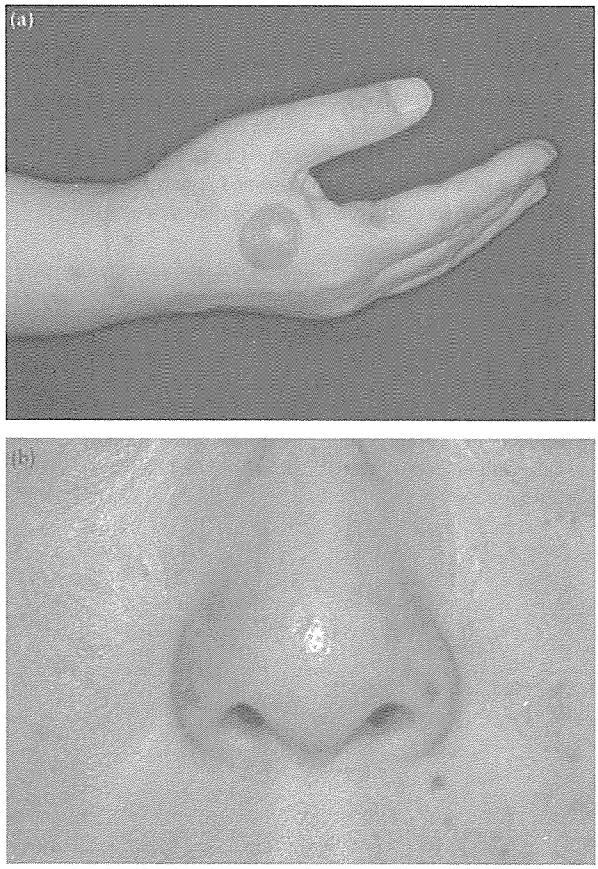

Figure 1 (a) Right hand with a tense blister, erosions and several pigmented lesions. (b) Numerous erosions on the face

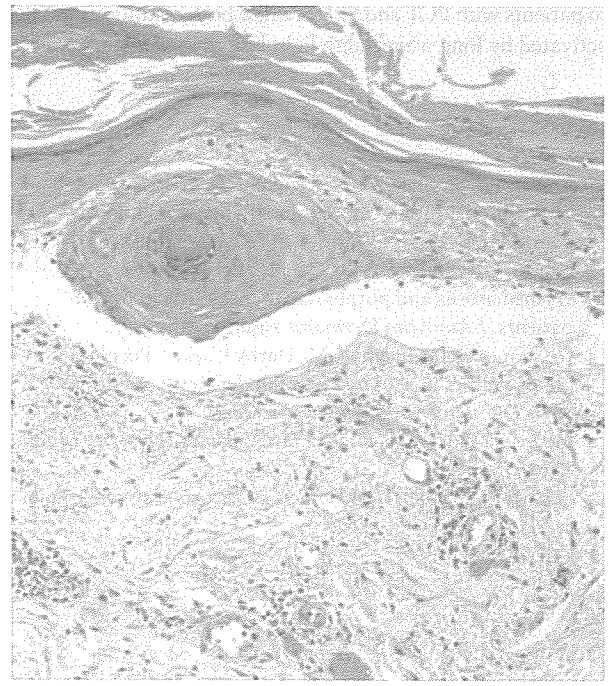

Figure 2 Subepidermal blister with slight inflammatory infiltrate. No eosinophilic deposits are observed around the vessels and few edematous changes were present in the dermis (H&E ×40)

decreased activity of uroporphyrinogen decarboxylase (UROD). Alcohol, oral contraceptives, polychlorinated hydrocarbons, disturbances of iron metabolism, hepatitis C and infection with HIV are recognized as precipitant factors for PCT.[3] Approximately 80% of PCT patients have the sporadic form in which UROD deficiency is restricted to the liver and the remainder has the familial type in which mutations in the UROD gene are inherited in an autosomal dominant pattern.[4]

It is not known whether the association between PCT and LE is coincidental or represents some common link. Harris *et al.* have suggested possible explanations for the coexistence of LE and porphyria: a common genetic abnormality, porphyria triggering an autoimmune response, preexisting LE resulting in an acquired metabolic fault leading to porphyria, and LE precipitating a genetically determined metabolic fault resulting in porphyria.[5] It is interesting that the gene for UROD is located on chromosome 1,[6] and that the 1q41–q42 region of that chromosome is probably linked to SLE.[7]

Our patient did not drink much alcohol, take oral contraceptives, nor had any blood transfusions. She did not have HCV or HIV infections. Her liver function test was abnormal, and therefore dysfunction of her liver caused by SLE may have been a factor in precipitating the PCT. She had suffered from hemolytic anemia since 1997, so an overload of iron may have caused liver dysfunction and could also have precipitated the PCT. The histological findings of the subepidermal blistering are compatible with PCT, and positive immunofluorescence staining at the DEJ may have been caused by the SLE and sun-exposed skin.

Association of SLE and PCT is not common, and this combination usually poses practical problems and occasionally therapeutic dilemmas. Phlebotomy is one treatment for PCT, but it is not advisable in LE patients who have anemia. Antimalarials are used for the treatment of LE and PCT. Severe toxicity can result from using high doses of chloroquine,[8] and hydroxichloroquine may also be associated with abdominal crises in some cases.[9] However, low-dose chloroquine therapy has been shown to be effective without causing serious hepatotoxicity.[10] Therefore, it is important to avoid high-dose chloroquine therapy in cases of joint LE and PCT.

Our patient's skin lesion and the quantity of porphyrines in her urine have been improved since she started the avoidance of sun exposure together with the topical steroid ointment treatment. Strict total sun protection should be recommended

to patients with PCT and SLE because both conditions can be activated by long wavelength light bound in sunlight.

References

1 Linden IH, Steffen CG, Newcomer VD, *et al.* Development of porphyria during chloroquine therapy for choronic discoid lupus erythmatosus. *Calif Med* 1954; 81: 235–238.
2 Gibson GE, McEvoy MT. Coexistence of lupus erythematosus and porphyria cutanea tarda in fifteen patients. *J Am Acad Dermatol* 1998; 4: 569–573.
3 O'Connor WJ, Murphy GM, Darby C, *et al.* Porphyrin abnormalities in acquired immunodeficiency syndrome. *Arch Dermatol* 1996; 132: 1443–1447.
4 Elder GH. Porphyriacutanea tarda. *Semin Liver Dis* 1998; 18: 67–75.
5 Harrris MY, Mills GC, Levin WC. Coexistent systemic lupus erythematosus and porphria. *Arch Intern Med* 1966; 117: 425–428.
6 Wu C, Xu W, Kozack CA, *et al.* Mouse uroporphyrinogen decarboxylase. cDNA cloning, expression, and mapping. *Mamm Genome* 1996; 7: 349–352.
7 Tsao BP, Cantor RM, Kalunion KC, *et al.* Evidence for linkage of a candidate chromosome I region for human systemic lupus erythematosus. *J Clin Invest* 1997; 99: 725–731.
8 Felsher BF, Redeker AG. Effect of chloroquine on hepatic uroporphrin metabolism in patients with porphyria cutanea tarda. *Medicine (Balt)* 1966; 45: 575–583.
9 Koranda FC. Antimalarials. *J Am Acad Dermatol* 1981; 4: 650–655.
10 Taljaard JJ, Shanley BC, Stewart-Wynne EG, *et al.* Studies on low dose choloroquine therapy and the action of chloroquine in symptomatic porphria. *Br J Dermatol* 1972; 87: 261–269.

eosinophils (816/μL). Blood chemistry values were normal except for lactate dehydrogenase level (331 IU/mL; normal range, 119-229 IU/mL). A skin biopsy specimen showed moderate perivascular infiltration of lymphocytes in the upper dermis with exocytosis into the epidermis (Figure). Most of the lymphocytes were CD4 positive. T-cell monoclonality, as assessed by Southern blot analysis of T-cell receptor Cβ1, was absent.

Aspirin therapy was discontinued, and he was treated with topical application of 0.1% mometasone furoate once a day for 2 months and narrowband UV-B irradiation (total dose, 19 600 mJ/cm^2) with clinical improvement. Although patch test results to the 2 drugs were negative, the lymphocyte stimulation test result was positive with aspirin, with a stimulation index of 4.48 (normal, <1.8). An oral challenge test result was positive with aspirin (20 mg, one fifth of the daily dose), as the patient developed the same erythematous papular eruption 24 hours after administration.

A flow cytometric analysis of the patient's peripheral blood lymphocytes was performed. The percentages of T_H1 and T_H2 cells were determined by the expression of chemokine receptors, CXCR3 and CCR4, respectively.[3] Twenty-four hours after the oral provocation test, the patient had a higher percentage of $CCR4^+$ $CD4^+$ T_H2 cells (36%) than $CXCR3^+$ $CD4^+$ T_H1 cells (8%). The percentage of $CD4^+$ cutaneous lymphocyte-associated antigen $(CLA)^+$ T cells was 12% at this time. After clinical improvement of the eruption, the percentages of $CCR4^+$ $CD4^+$ T_H2 cells and $CD4^+$ CLA^+ T cells were decreased to 28% and 1%, respectively. No recurrence was observed 14 months after cessation of aspirin.

Comment. Although the pathogenesis of papuloerythroderma remains unclear, a reaction to an unidentified cutaneous antigen has been suggested as well as the association with neoplasia.[2] Our case clearly demonstrated that aspirin can cause this eruption. The similar histologic findings to this case has been reported to be caused by other drugs under the title of pseudomycosis fungoides.[4,5] The known relationship of papuloerythroderma with mycosis fungoides further suggests that drugs are causative agents for papuloerythroderma.

Kazunari Sugita, MD
Chizuko Koga, MD
Ryutaro Yoshiki, MD
Kunio Izu, MD
Yoshiki Tokura, MD

Correspondence: Dr Sugita, Department of Dermatology, University of Occupational and Environmental Health, Japan, 1-1 Iseigaoka, Yahatanishi-ku, Kitakyushu 807-8555, Japan (k-sugita@med.uoeh-u.ac.jp).
Financial Disclosure: None.

1. Ofuji S, Furukawa F, Miyachi Y, Ohno S. Papuloerythroderma. *Dermatologica.* 1984;169:125-130.
2. Wakeel RA, Keefe M, Chapman RS. Papuloerythroderma: another case of a new disease. *Arch Dermatol.* 1991;127:96-98.
3. Shimauchi T, Imai S, Hino R, Tokura Y. Production of thymus and activation-regulated chemokine and macrophage-derived chemokine by CCR4+ adult T-cell leukemia cells. *Clin Cancer Res.* 2005;11:2427-2435.
4. Gordon KB, Guitart J, Kuzel T, et al. Pseudo-mycosis fungoides in a patient taking clonazepam and fluoxetine. *J Am Acad Dermatol.* 1996;34:304-306.
5. Vermeer MH, Willemze R. Is mycosis fungoides exacerbated by fluoxetine? *J Am Acad Dermatol.* 1996;35:635-636.

Mycosis Fungoides Bullosa

Mycosis fungoides (MF), a cutaneous lymphoma with diverse clinical manifestations, rarely presents with vesiculobullous lesions, or MF bullosa (MFB). Mycosis fungoides with large cell transformation, transformed MF (T-MF), is also another rare condition. We report 2 cases of MFB, one of which was complicated with T-MF.

Report of Cases. *Case 1.* A 72-year-old woman, who was first diagnosed as having MF in her fifties (**Figure 1**A and B), presented with multiple nodules on her back (Figure 1C). Skin specimens of a nodule showed atypical cells with enlarged, pale nuclei clustered in the dermis (Figure 1D).These malignant cells stained positive for CD30. She was diagnosed as having T-MF and was treated with psoralen plus UV-A (PUVA) and topical corticosteroids.

At age 82 years, she presented with asymptomatic blisters measuring up to 10 mm in diameter, which were scattered over her right thigh (Figure 1E). She denied any history of insect bites, drug use, burns, or contact allergy. Within 5 months, the blisters resolved. A skin biopsy specimen from a blister revealed that the epidermis was separated from the dermis, and a bandlike infiltration of cells was seen (Figure 1F). The infiltrate was mainly composed of small atypical lymphocytes, intermingled with few histiocytes and eosinophils. Findings from immunohistochemical analysis showed that the infiltrate was predominantly composed of T cells (CD3 positive and CD30 negative). No large cells corresponding to T-MF were observed. Immunofluorescence revealed the absence of circulating autoantibodies against epidermis and no deposition of immunoglobulins and complements in vivo. We diagnosed the blistering lesions as MFB. The lesions disappeared after topical corticosteroid treatment and have not reappeared in the subsequent 2 years. She is still alive with lymph node and visceral involvement of MF.

Case 2. A 50-year-old woman with a 40-year history of early-stage MF visited our hospital after progression to tumor stage with multiple tumors over her whole body (**Figure 2**A). She was treated with topical corticosteroids, total electron beam irradiation, and 3 cycles of cyclophosphamide, doxorubicin hydrochloride, vincristine sulfate, and prednisone (CHOP) chemotherapy. Two months before her death, several vesicles appeared on her trunk (Figure 2B). She denied a history of insect bites, drug use, burns, or contact allergy. Histopathological findings from the vesicle showed subepidermal bulla with bandlike infiltration of atypical lymphocytes in the upper dermis (Figure 2C). She died of infection secondary to ulceration of tumor sites.

Comment. Bowman et al[1] proposed the following criteria for MFB diagnosis: (1) clinically apparent vesiculobullous lesions, (2) typical histologic features of MF with blisters, (3) negative immunofluorescence findings, and (4) exclusion of other causes of vesiculobul-

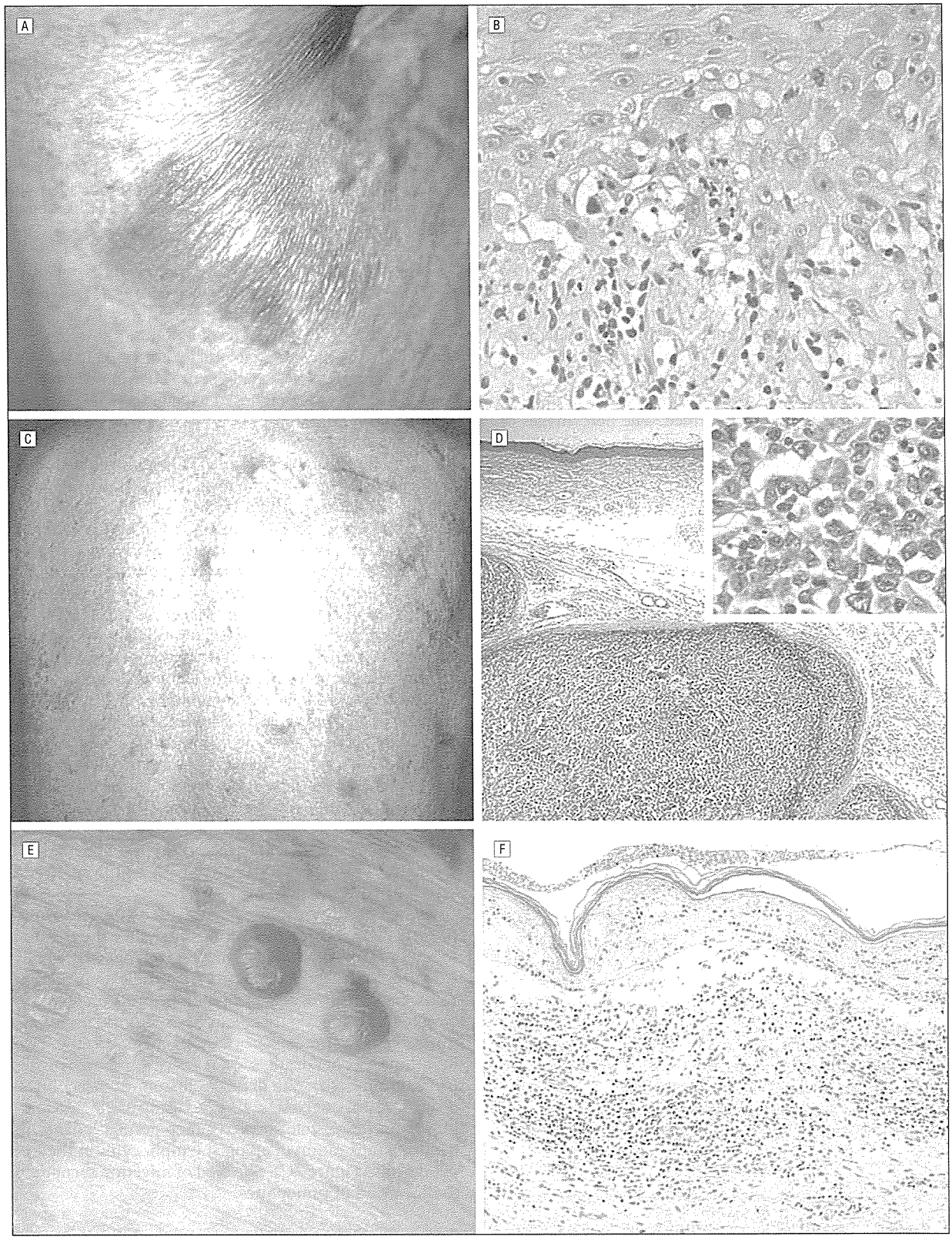

Figure 1. Case 1. A, Dark reddish macules on the trunk corresponding with typical mycosis fungoides. B, A bandlike upper dermal infiltrate with epidermotropism of small atypical lymphocytes (hematoxylin-eosin, original magnification ×400). C, Multiple nodules on her back. D, Tumor cells from nodule are located intradermally (hematoxylin-eosin, original magnification ×50). Atypical cells are large and have an abundant cytoplasm (hematoxylin-eosin, original magnification ×400) (inset). Those cells are CD30 positive. E, Blisters are seen on her right thigh. F, Subepidermal bullae are seen with atypical lymphocytes (hematoxylin-eosin, original magnification ×100).